PY5021 - 4 Sensor Types (I)

J. M. D. Coey

School of Physics and CRANN, Trinity College Dublin

Ireland.

1. Induction sensors
2. Semiconductor sensors
3. Thin film magnetic sensors

Comments and corrections please: jcoey@tcd.ie

www.tcd.ie/Physics/Magnetism

Sensor Types (I)

4.1 Induction sensors.
Search coil, sensitivity. Fluxgates, core designs, numerical analysis of a fluxgate, miniaturization. Ilustration of space-borne and laboratory instruments

4.2 Semiconductor sensors
Classical B^2 magnetoresistance, analysis of multiband MR in terms of mobility. InAs, InSb. Hall effect. Silicon, Integrated Hall sensors. InAs 2deg sensors. Magnetodiodes and magnetotransistors.

4.3 Thin-film magnetic sensors
AMR effect. AMR sensor design, commercial AMR bridges. GMR effect, GMR sensor stacks, exchange bias, sensitivity, crossed anisotropy, GMR sensor design, high-frequency response, CIP and CPP GMR. TMR effect, TMR sensor stacks, AlO_x and MgO barriers, coherent and incoherent tunneling, TMR sensor design considerations, resistance, sensitivity, high-frequency response. GMI effect. Implementation of GMI sensors as wires and thin films. Commercial 3-axis GMI sensors.

Sensor	Principle	Detects	Frequency	Field (T)	Noise	Comments
Coil	Faraday's law	dΦ/dt	10^{-3} - 10^{9}	10^{-10} - 10^{2}	100 nT	bulky ,absolute
Fluxgate	saturation	H	dc - 10^{3}	10^{-10} - 10^{-3}	10 pT	bulky
Hall probe	Lorentz f'ce	B	dc - 10^{5}	10^{-5} - 10	100 nT	thin film
MR	Lorentz f'ce	B^2	dc - 10^{5}	10^{-2} - 10	10 nT	thin film
AMR	spin-orbit int	H	dc - 10^{7}	10^{-9} - 10^{-3}	10 nT	thin film
GMR	spin accum.n	H	dc - 10^{9}	10^{-9} - 10^{-3}	10 nT	thin film
TMR	tunelling	H	dc - 10^{9}	10^{-9} - 10^{-3}	1 nT	thin film
GMI	permability	H	dc - 10^{4}	10^{-9} - 10^{-2}		wire
MO	Kerr/Faraday	M	dc - 10^{5}	10^{-9} - 10^{2}	1 pT	bulky
SQUID lt	flux quanta	Φ	dc - 10^{9}	10^{-15} - 10^{-2}	1 fT	cryogenic
SQUID ht	flux quanta	Φ	dc - 10^{4}	10^{-15} - 10^{-2}	30 fT	cryogenic
NMR	resonance	B	dc - 10^{3}	10^{-10} - 10	1 nT	Very precise

4.1 Induction sensors

4.1.1 Search coil

Inductive sensors detect an emf in a coil proportional to the rate of change of flux, according to Faraday's law:

$$\mathcal{E} = -d\Phi/dt$$

A search coil with n turns of area $\mathcal{A}$, is removed from a region where the field is B' to an region where the field is ≈ 0. $n dB\mathcal{A}/dt = \mathcal{E}$; $n\mathcal{A}\int_0^{B'} dB = n\mathcal{A}B' = \int_0^{\infty} \mathcal{E}\, dt = \int_0^{\infty} IR dt = R\int_0^{Q} dq = RQ$ where total Q is the total charge passed, measured with an integrating voltmeter.

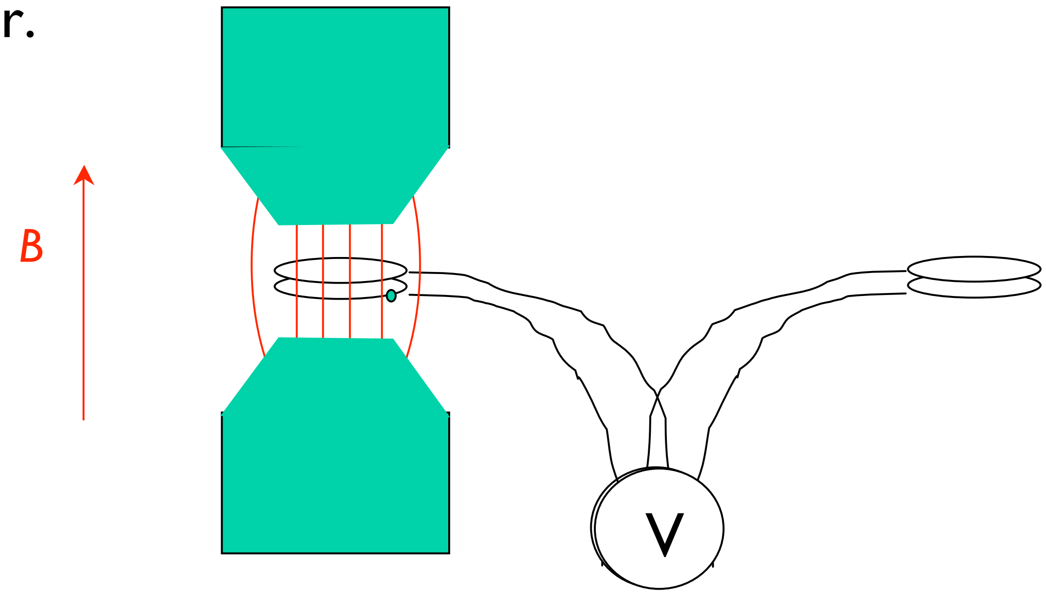

4.1.2 Rotating coil fluxmeter

Again:

$$\mathcal{E} = -d\Phi/dt$$

A search coil with n turns of area $\mathcal{A}$, is rotated at frequency f

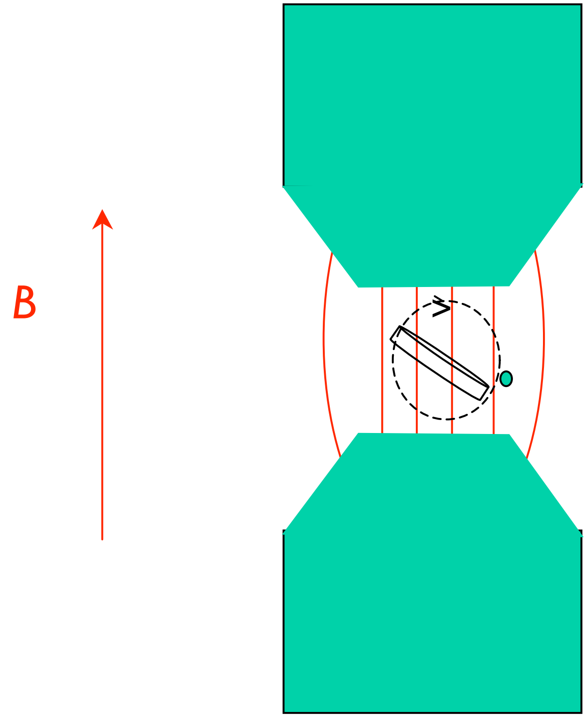

$\mathcal{E}(t) = n\mathcal{A}B \cos 2\pi f t$

Operates at ~ 100 Hz

Use lockin detection to measure a uniform field, in a narrow bandwidth of Johnson noise around f.

Ignore L, C.

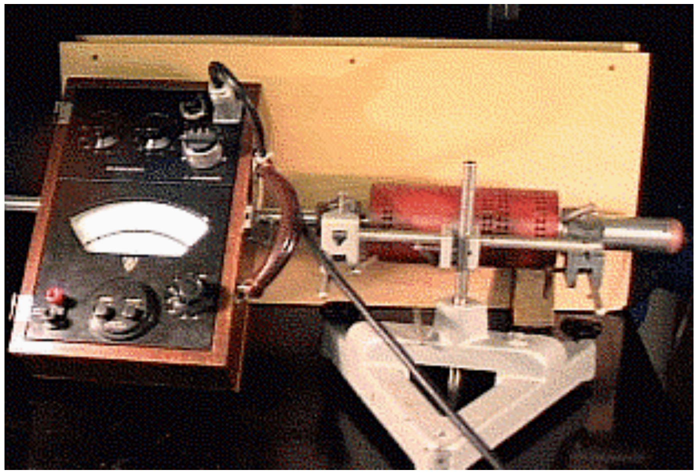

4.1.3 Inductive heads

Inductive read/write heads were widely used until 1990 in magnetic recording

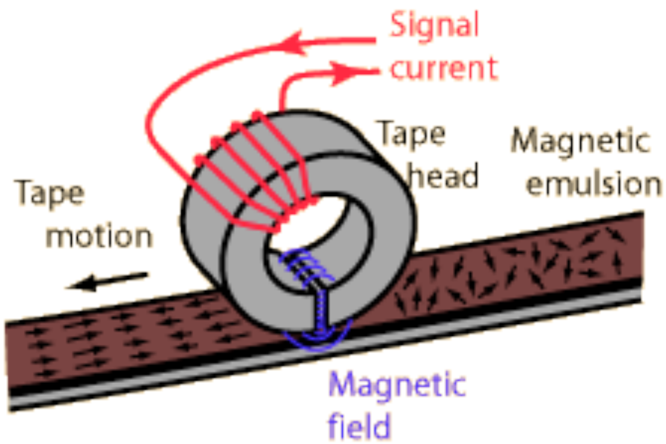

The magnetic circuit is often composed of an insulating soft ferrite ring (soft iron is unsuitable unless it is made of very thin laminations because of the eddy currents that would be induced at high data rates).

read/write head

$$\oint H d\ell = nI$$

If the yoke has a very high relative permeability, the *H*-field in the soft material is negligible, and the only contribution to the integral comes from the airgap. $H_g g = nI$

In general the deep gap field $H_g = \varepsilon nI/g$

ε is < 1, to take account of core flux loss.

Provided z > 0.2g the field is given by the Karquist equations

$$H_x = (H_g/\pi)\{\tan^{-1}[(g/2 + x)/z] + \tan^{-1}[(g/2 - x)/z]\}$$

$$H_z = (H_g/2\pi)\ \ln \{[(g/2 - x)^2 + z^2]/[(g/2 + x)^2 + z^2]\}$$

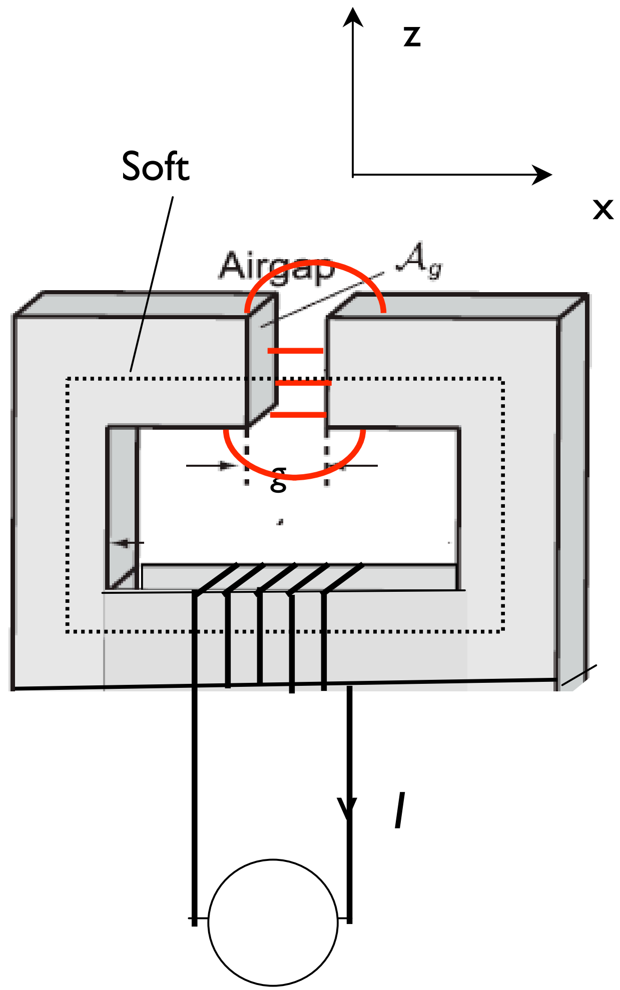

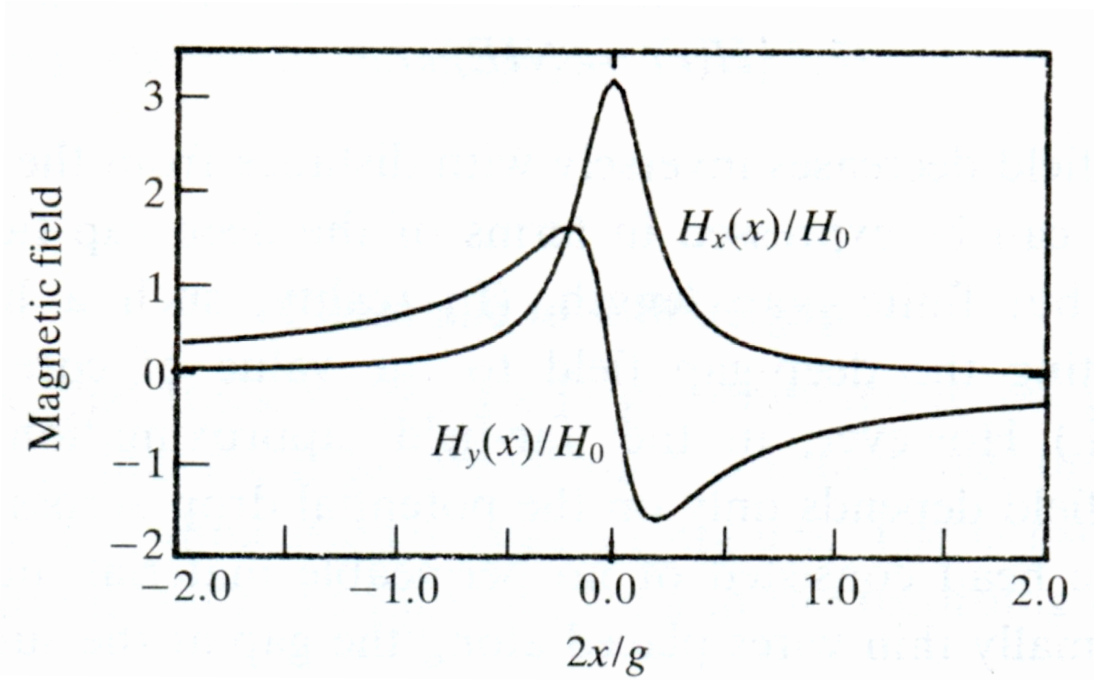

Used as a sensor, the inductive head is an efficient flux collector, which is concentrated through the head windings. The flux can be calculated by reciprocity as

$$\Phi(x) = (\mu_0/I)\int \boldsymbol{H}(r' + x).\boldsymbol{M}(r')\, d^3r' \qquad (1)$$

where $\boldsymbol{M}(x)$ is the magnetization pattern of the medium and $\boldsymbol{H}$ is the field produced by the head when a current I is passed.

$d\Phi/dt$ gives the induced emf in the coil.

4.1.4 Fluxgates

Fluxgates depend on the nonlinear saturation of the magnetization of a soft magnetic core in an ac field. Two identical cores (or a single bar or toroidal core) have oppositely wound ac field windings. A parallel applied field leads to longer saturation of one of the cores, producing an ac signal at twice the frequency, linear in H.

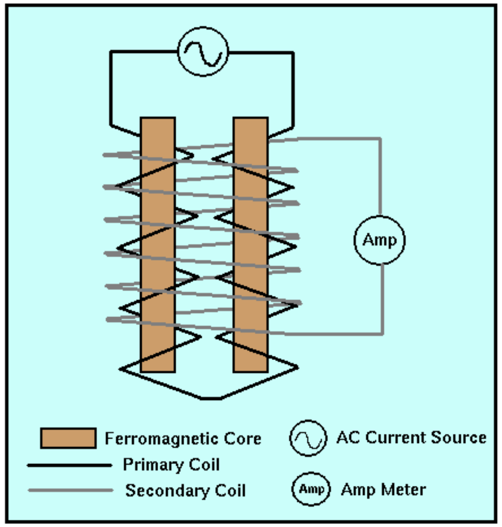

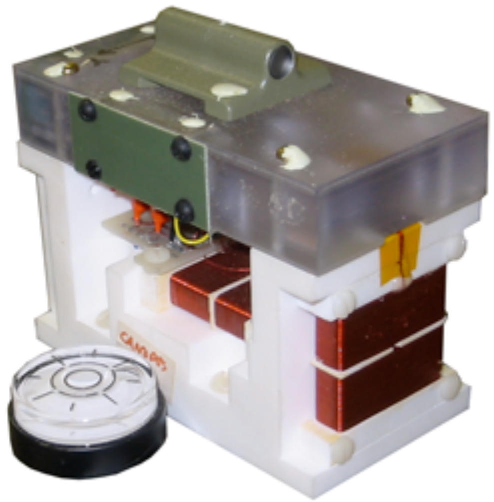

Fluxgates are bulky but sensitive, reliable and impervious to radiation. Used, for example, in space.

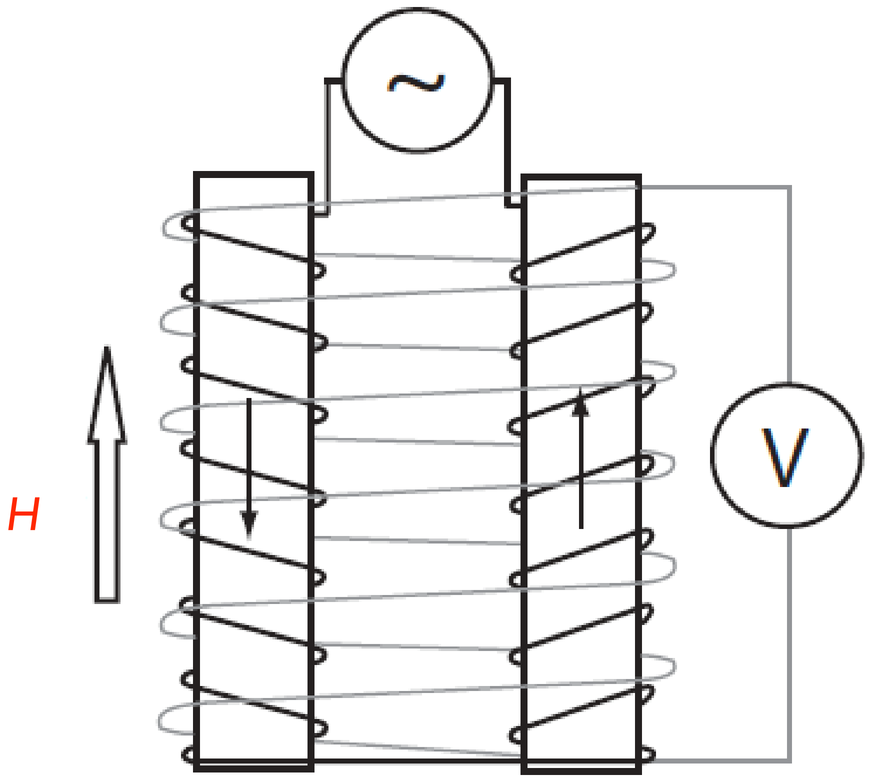

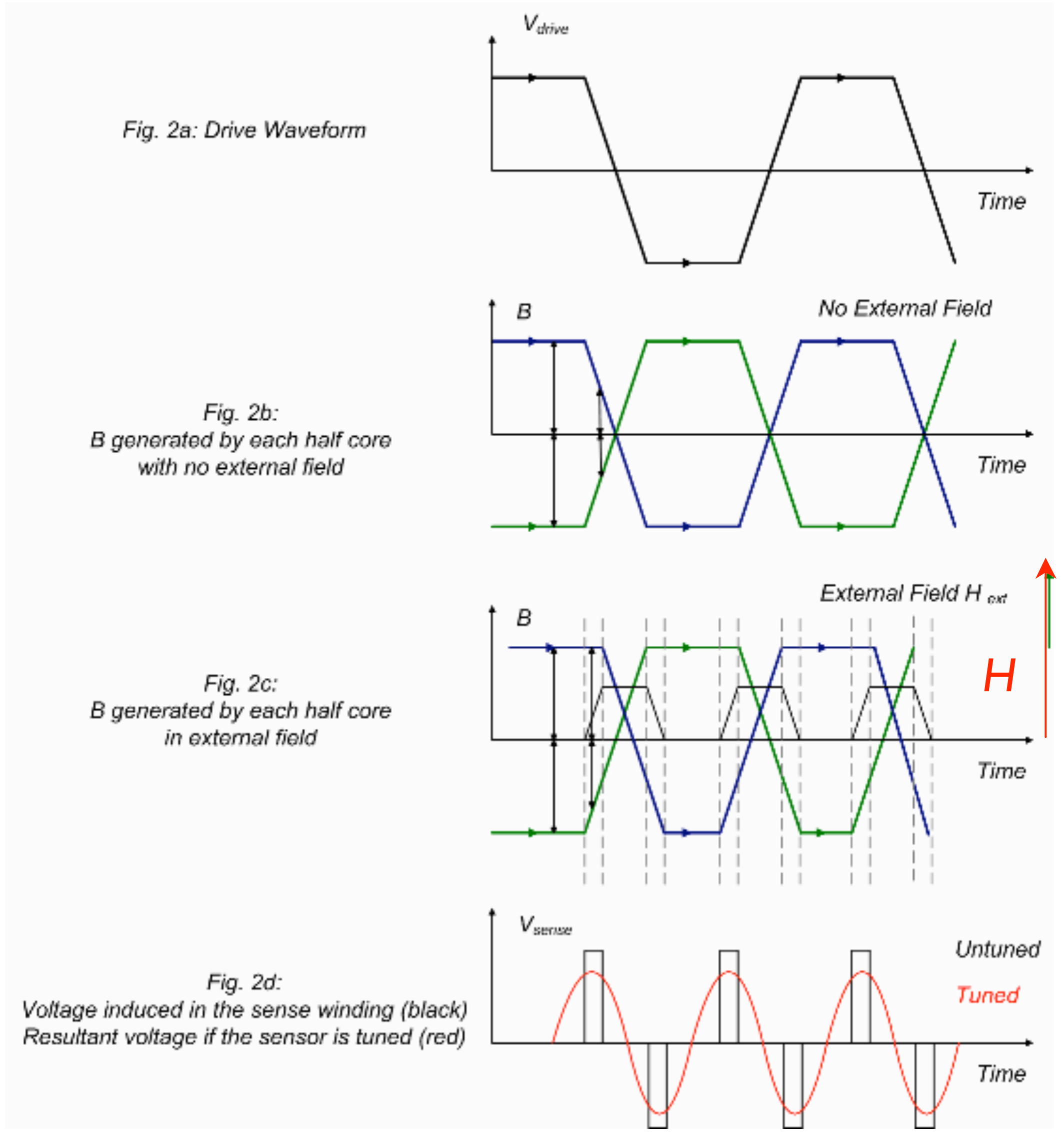

The ac saturation field is ~ 10 kHz

The signal at 2*f* is detected using a lock-in detector; Alternatively, the output can be used in a null field mode with a coil to compensate the external field. Pairs of fluxgates are used as gradiometers

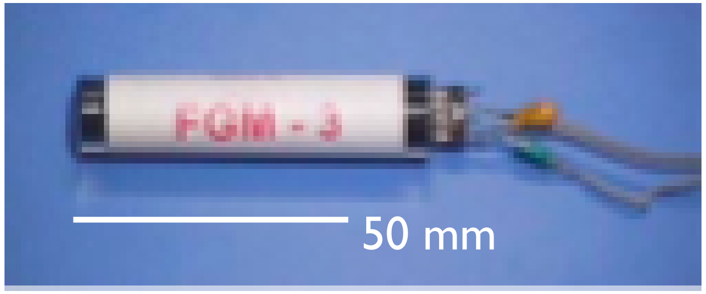

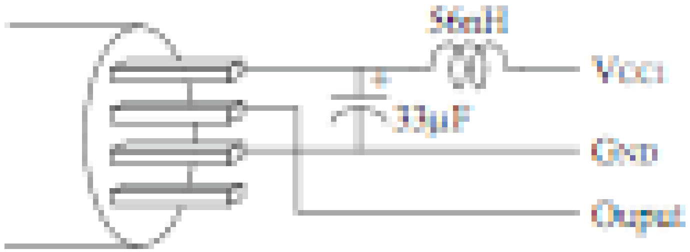

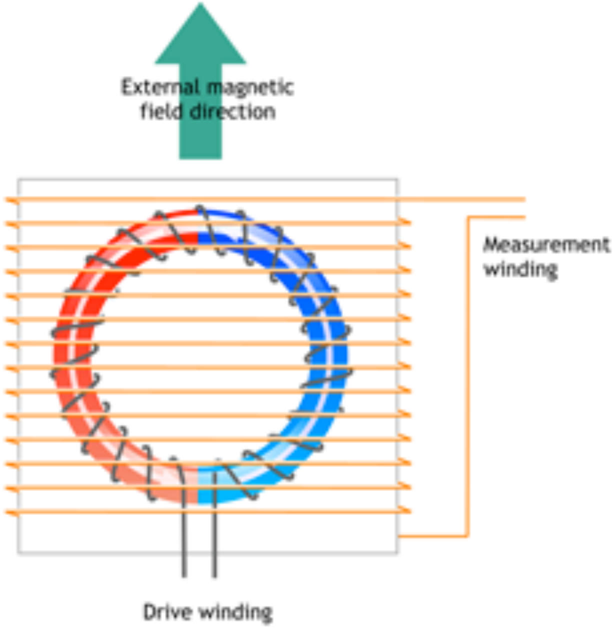

$$\boldsymbol{H \approx H' - \mathcal{N}M}$$

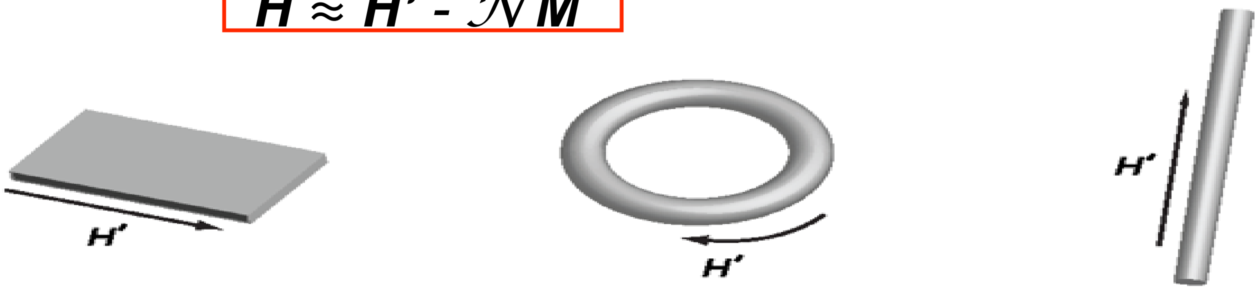

Core designs with $\mathcal{N} \approx 0$.

Use permalloy, with χ > 10,000 for ease of saturation. Typical range 0 - 50 μT, Sensitivity $\leq$ 1 nT.

4.2 Semiconductor sensors

4.2.1 Classical magnetoresistance

The simplest Lorentz force device is a semicoductor or semimetal which exhibits classical positive B^2 magnetoresiatance. High-mobility semiconductors such as InAs and InSb show large effects (~ 100 % T^{-1}). Field is applied perpendicular to the semiconductor slab, and it is possible to achieve a desired resistance by patterning a series of metallic contacts. Electrons must complete part of a cyclotron orbit before scattering. $\omega_c\tau > 1$. There is no effect for the free-electron gas; interband scattering is essential.

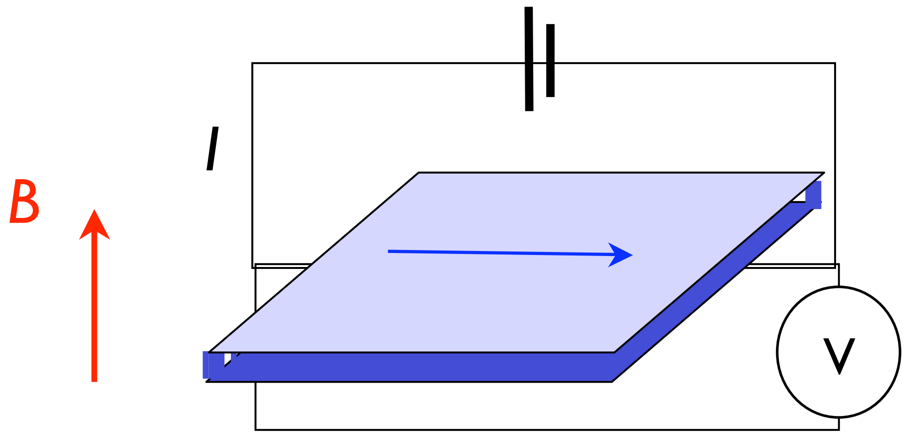

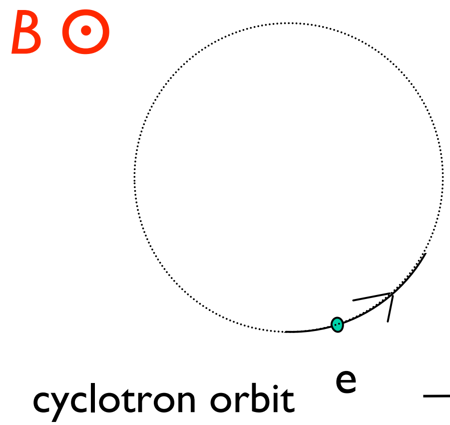

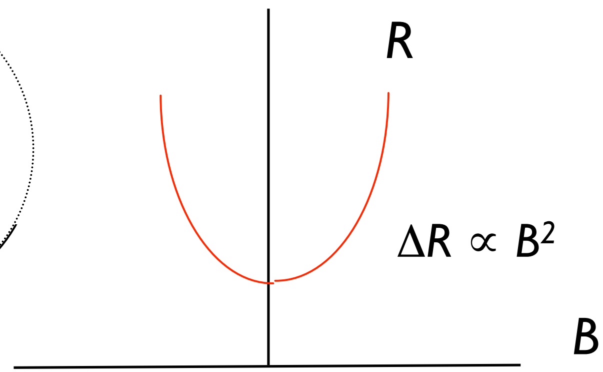

The sensors are nonlinear, two-terminal devices providing a good response in large fields. They have been used as position sensors in brushless dc permanent magnet motors.

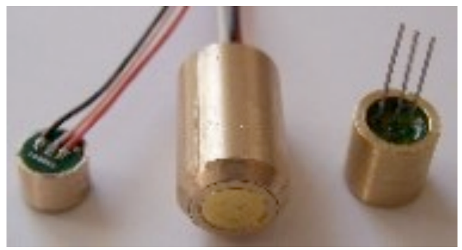

4.2.2 Hall effect

Effect discovered by Edwin Hall in 1879

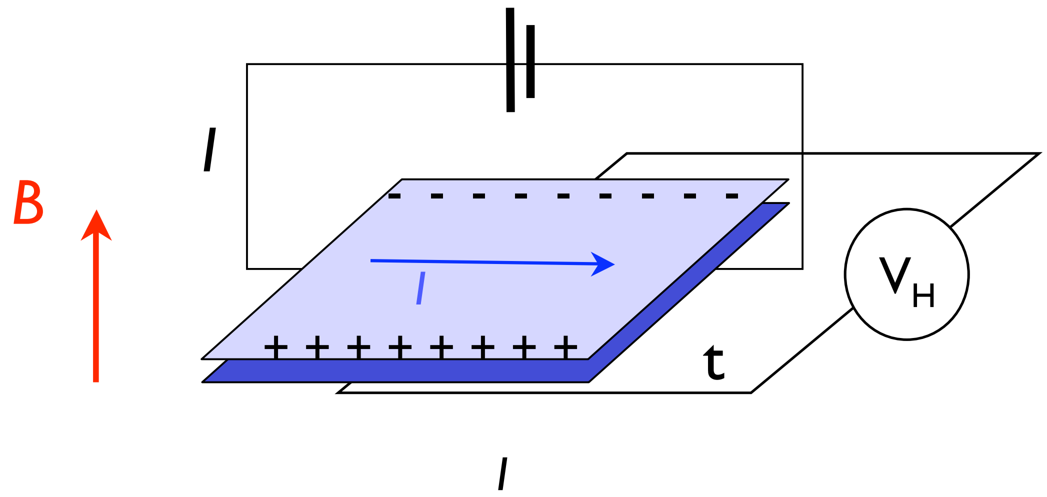

$$\boldsymbol{F} = q(\boldsymbol{E} + \boldsymbol{v} \times \boldsymbol{B})$$

$$V_H/t = R_0 jB \qquad R_0 = (1/ne)$$

$$E/j = \rho_{xy} = R_0 B$$

Hall voltages linear in field are produced in semiconductor plates, especially Si and in 2-deg GaAs/GaAlAs structures. These are four-terminal devices, and the current source and high-gain amplifier are often integrated on a chip.

Used for secondary field measurements – each probe must be calibrated — and as proximity sensors. About two billion are produced each year.

proximity switches

geartooth sensor

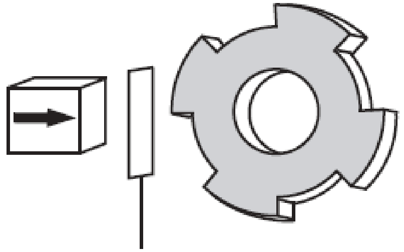

Variable-reluctance sensor based on a permanent magnet.

voltage sensor

current sensor

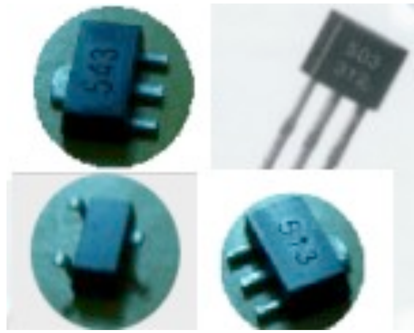

Hall ICs

Resistivity tensor for isotropic material in a magnetic field:

ρ_{xx}	$-\rho_{xy}$	0
ρ_{xy}	ρ_{yy}	0
0	0	ρ_{zz}

ρ_{xy} is the Hall resistivity.

$$\rho_{xy} = \mu_0(\underbrace{R_0H}_{\text{Normal Hall effect}} + \underbrace{R_mM}_{\text{Anomalous Hall effect}})$$

4.3 Thin film ferromagnetic sensors

4.3.1 Anisotropic magnetoresistance (AMR)

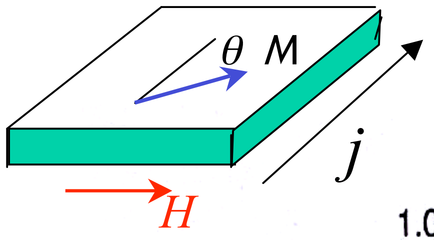

thin film

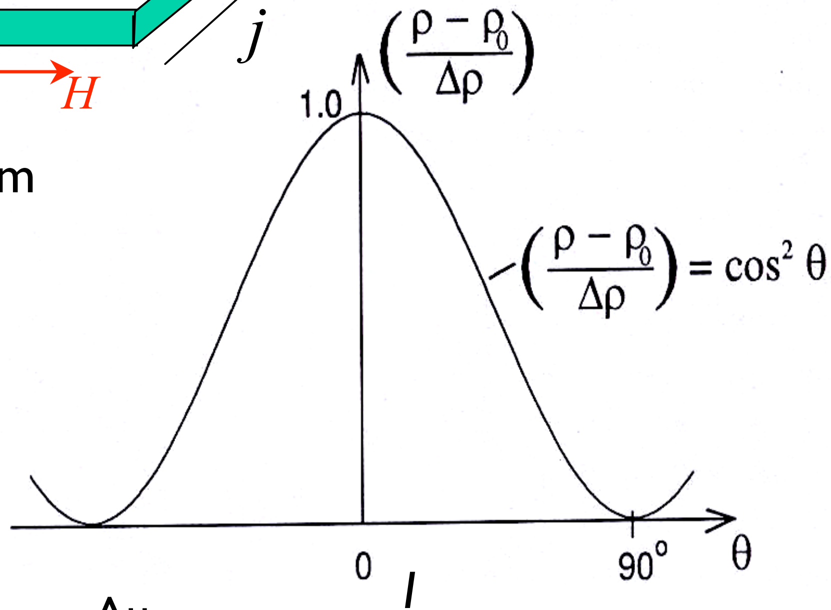

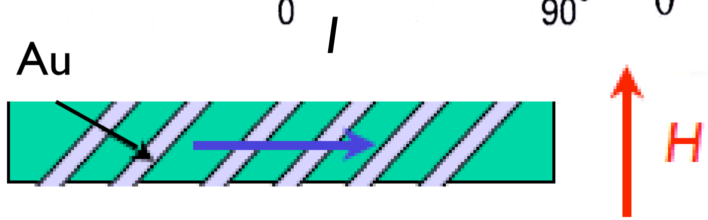

Barber pole

Discovered by W. Thompson in 1857

$$\boxed{\rho = \rho_0 + \Delta\rho \cos^2\theta}$$

Magnitude of the effect $\Delta\rho/\rho < 3\%$ The effect is usually positive; $\rho_{||} > \rho_{\perp}$

AMR is due to spin-orbit *s-d* scattering

High field sensitivity is achieved in thin films of soft ferromagnetic films such as permalloy ($Fe_{20}Ni_{80}$).

Soft adjacent layer (SAL) magnetized by the sense current in the AMR film, creates a stray field H_{sal}

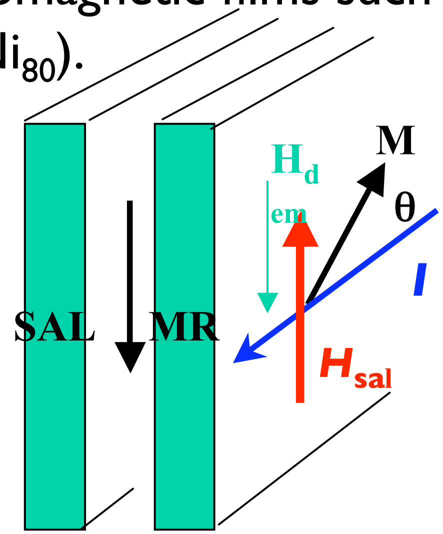

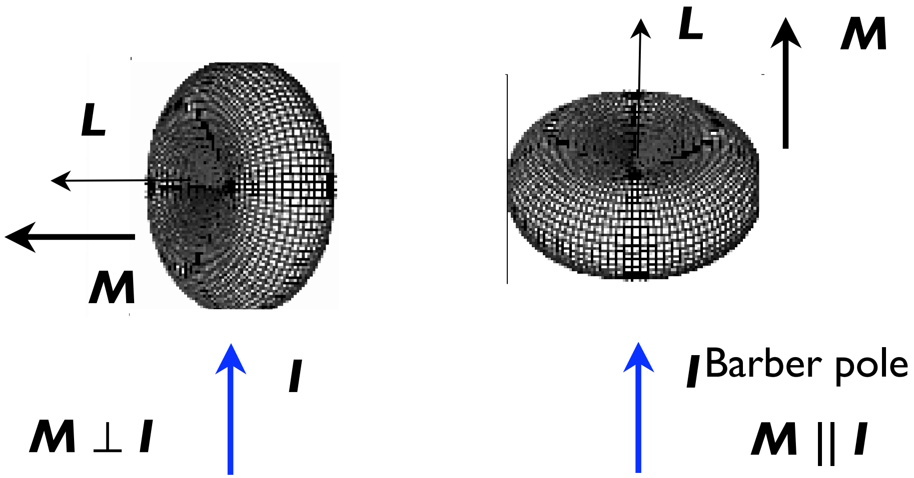

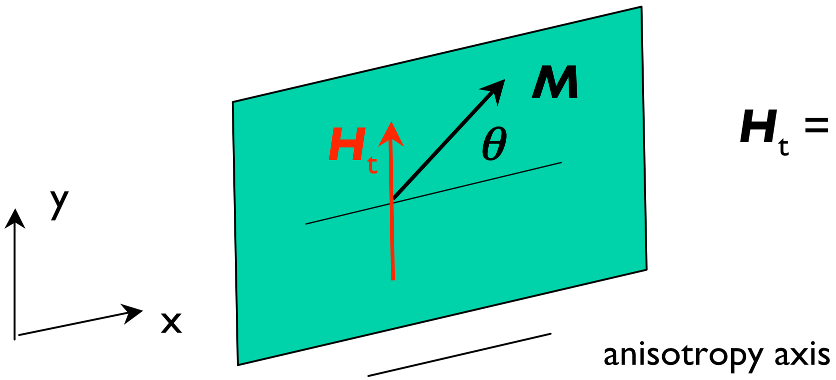

$\boldsymbol{H}_t = \boldsymbol{H} + \boldsymbol{H}_{sal}$

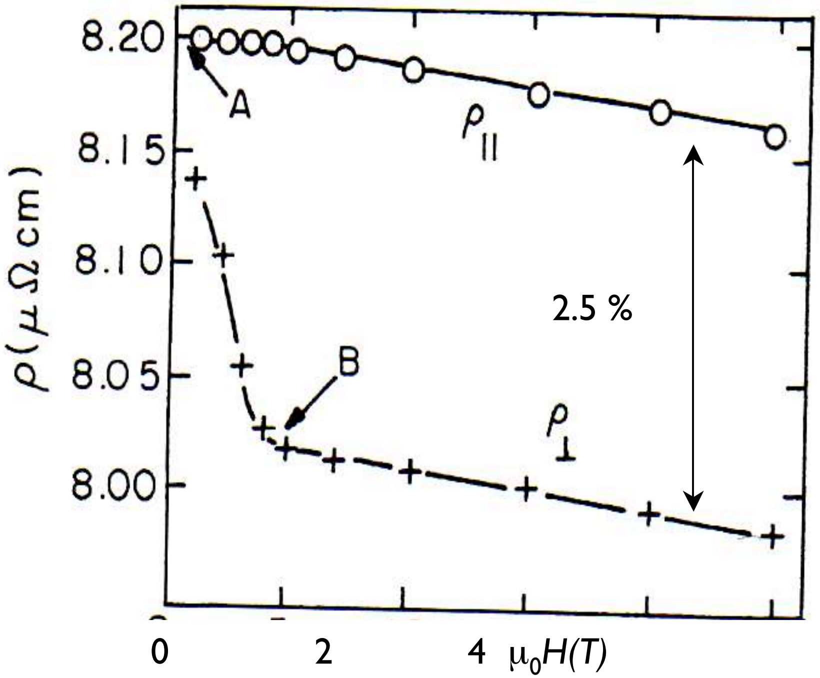

AMR of permalloy

The anisotropic magnetoresistance is due to spin-orbit scattering, $\rho_{\parallel} > \rho_{\perp}$.

$E = -\mu_0 H_t M\sin\theta + K_u \sin^2\theta - (1/2)\mu_0 H_d M\sin\theta$ where $H_d = -\mathcal{N}_y M\sin\theta$

$\sin\theta = \mu_0(H + H_{sal})/[2K_u + \mu_0\mathcal{N}_y M^2]$ assuming $\boldsymbol{M}$ is uniform over the film

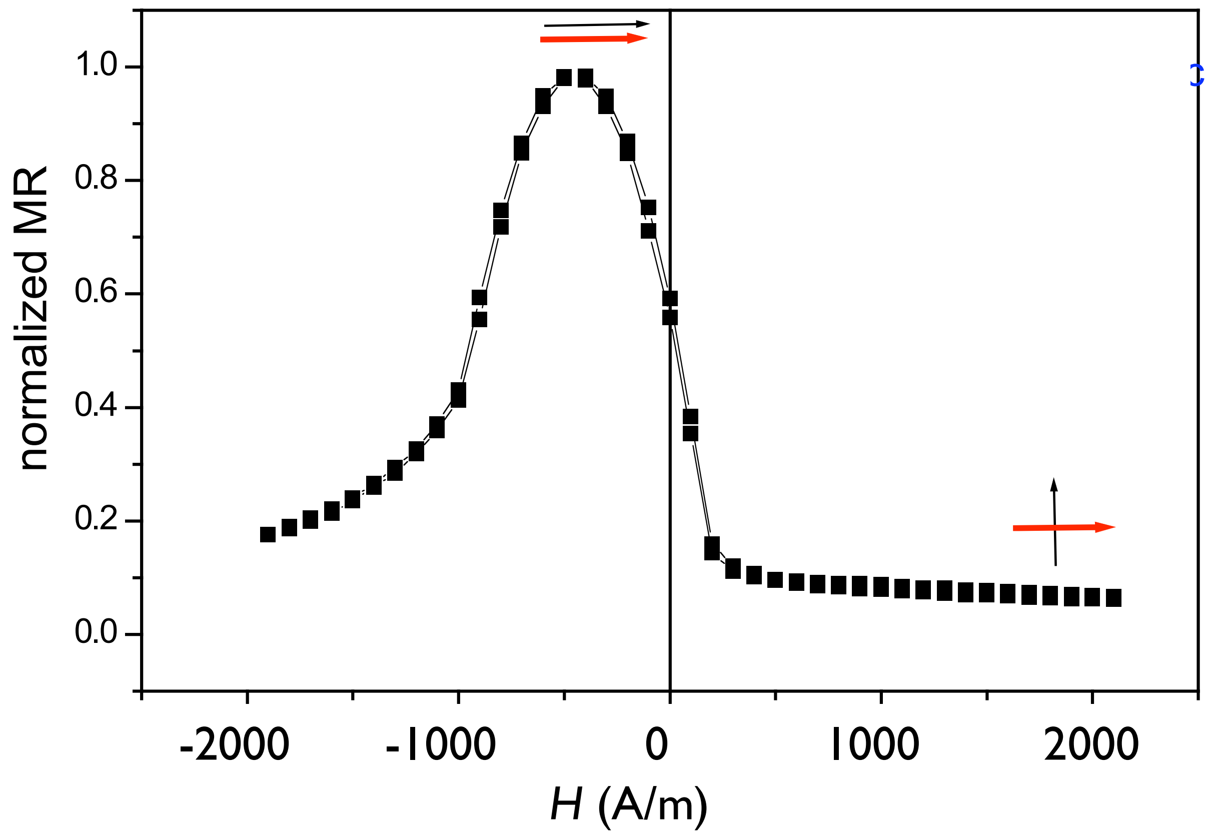

Note: 1. The response is linear around zero sense field.

2. Very large current densities (~ 10^{11} A/m^2) are needed to bias the SAL.

4.2.2 Planar Hall effect

Planar Hall effect is a variant of AMR; $\rho_{||} \neq \rho_{\perp}$ $\rho_{||}$ is when $j \parallel M$ ….

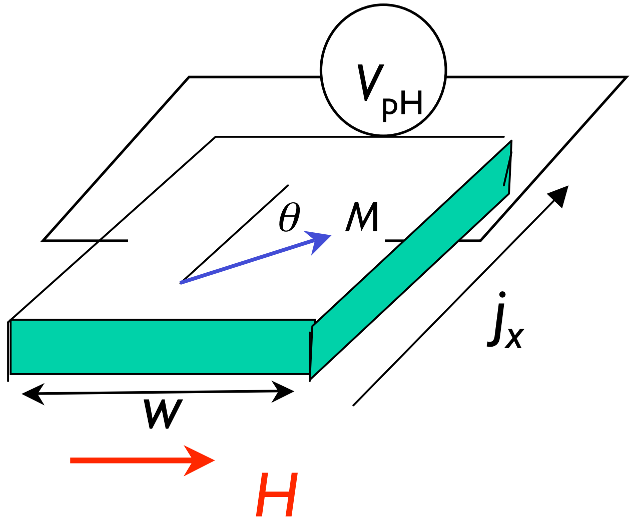

$E_{||} = \rho_{||}\, j_x \cos\theta \qquad E_{\perp} = \rho_{\perp} j_x \sin\theta$

Components of electric field parallel and perpendicular to the current are

$E_x = E_{||}\cos\theta + E_{\perp}\sin\theta, \qquad E_y = E_{||}\sin\theta - E_{\perp}\cos\theta$

$E_x = j(E_{||}\rho_{\perp} + \Delta\rho\cos^2\theta) \qquad E_y = j\,\Delta\rho\,\sin\theta\,\cos\theta$

Hence

$$\boxed{V_{pH} = j\, w\Delta\rho\, \sin\theta\, \cos\theta}$$

The biggest effect is when θ changes from 45 to 135 degrees. Since $\sin\theta \propto H$, $V_{pH} \approx H$

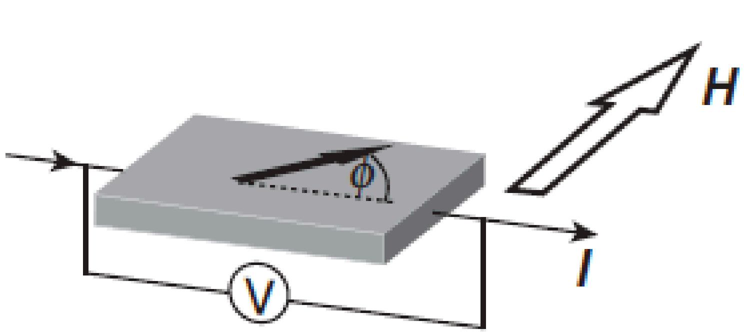

AMR

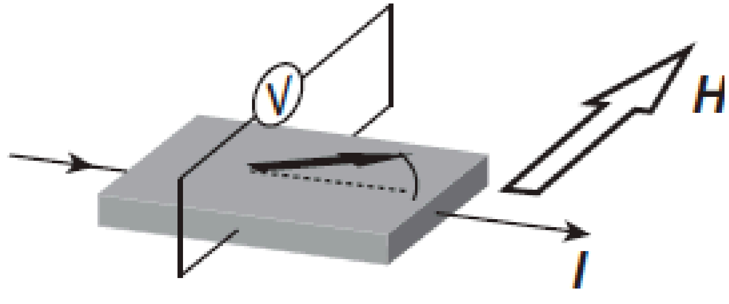

Planar Hall effect

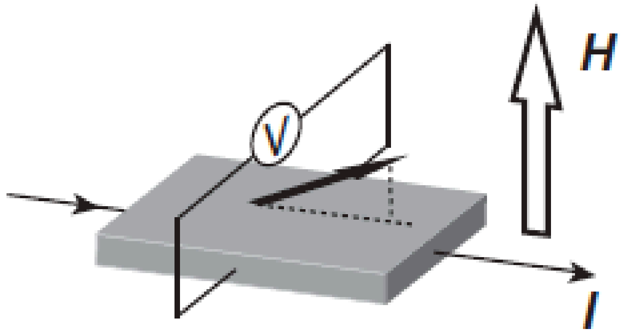

Anomalous Hall effect

4.3.3 Giant magnetoresistance.

Peter Grunberg and Albert Fert;

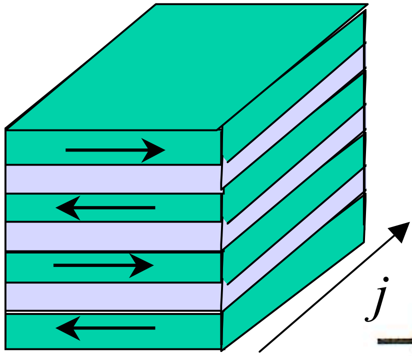

Fe/Cr stack

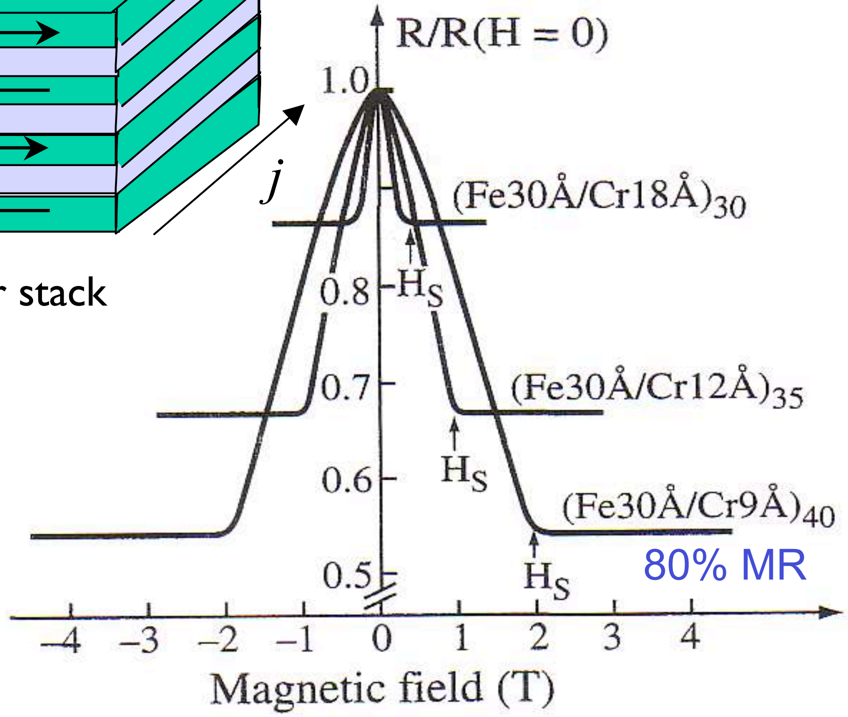

10^9 GMR sensors per year

Discovery of GMR 1988

Implementation in hard disk drives 1998

Nobel Prize 2007

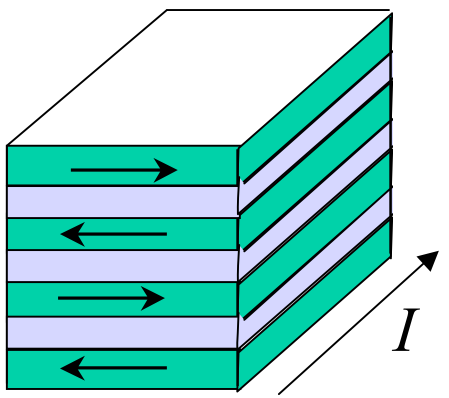

thin film stack

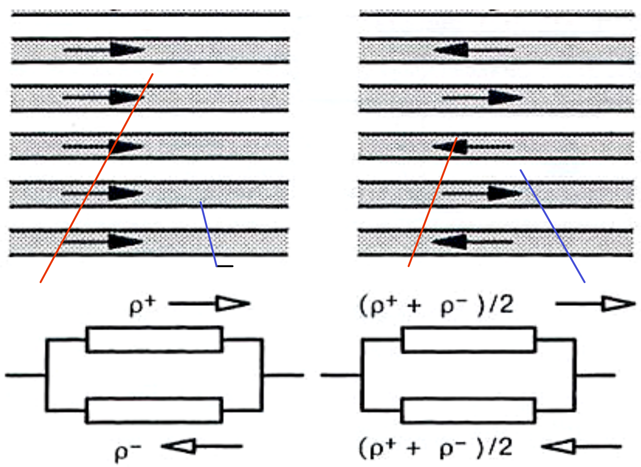

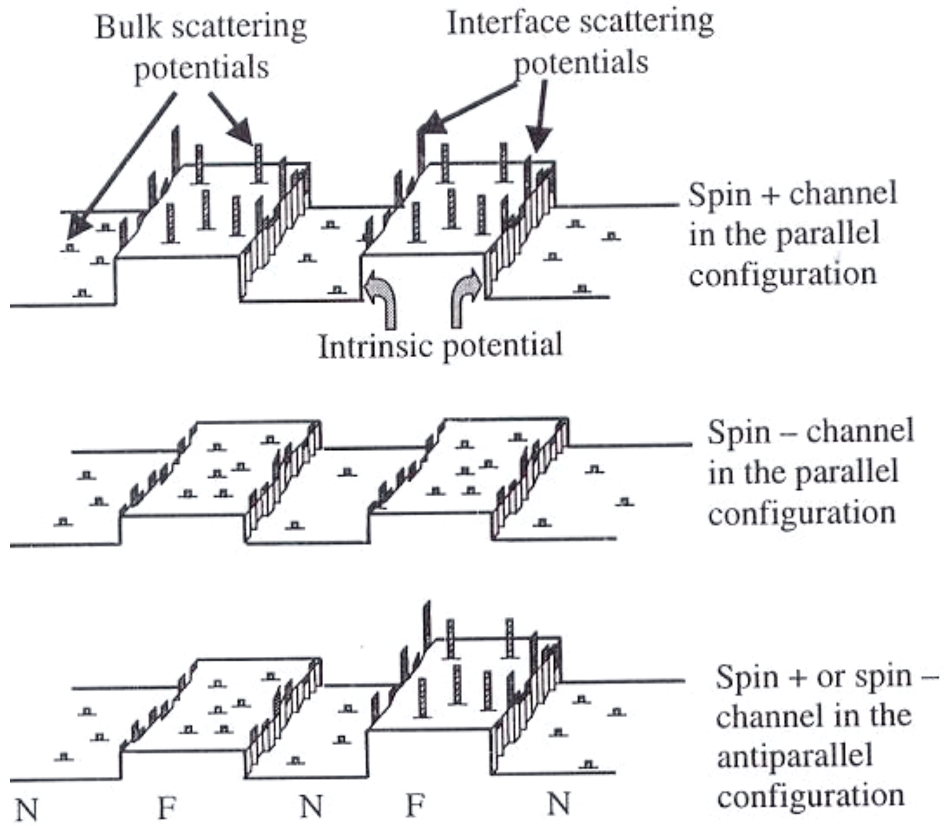

$$MR = (\alpha^2 - 1)/4\alpha$$

Mott's Two-current model. Distinct resistancer parallel ↑ and ↓ current flows.

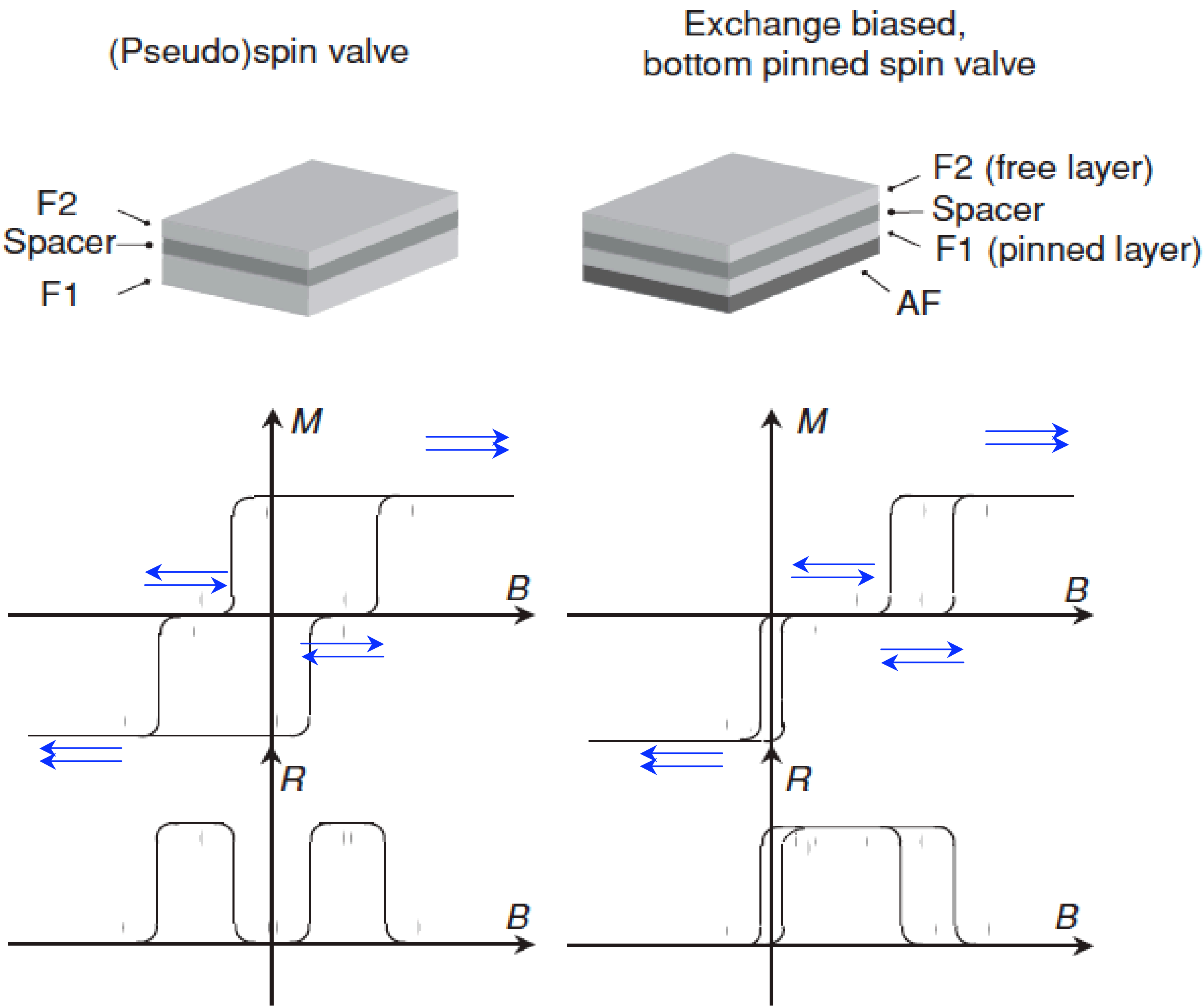

(Pseudo)spin valve
Exchange biased,
bottom pinned spin valve
F2
Spacer
F1
F2 (free layer)
Spacer
F1 (pinned layer)
AF
M
B
R
B
M
B
R
B

Spin valve

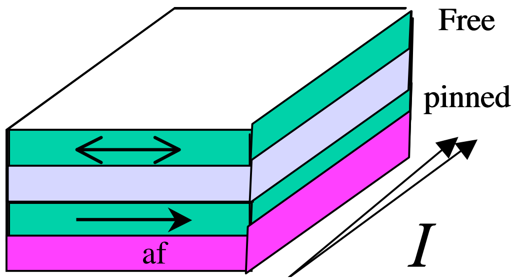

GMR spin valve

Exchange-biased stack

$$MR_{max} = \frac{(R_{ap} - R_p)}{R_p} = \frac{(G_p - G_{ap})}{G_{ap}}$$

Exchange Bias.

Discovered by Mieklejohn and Bean; 1956 *'A new type of magnetic anisotropy has been discovered, which is best described as exchange anisotropy. This anisotropy is a result of an interaction between an antiferromagnetic material and a ferromagnetic material'*

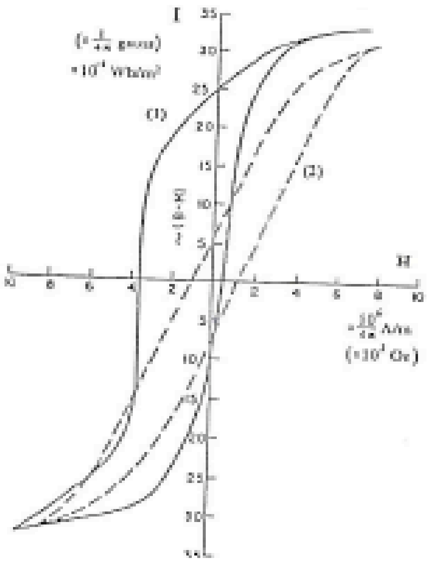

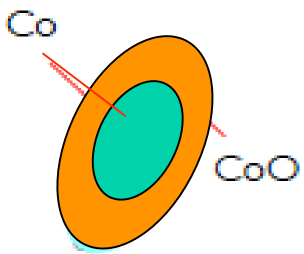

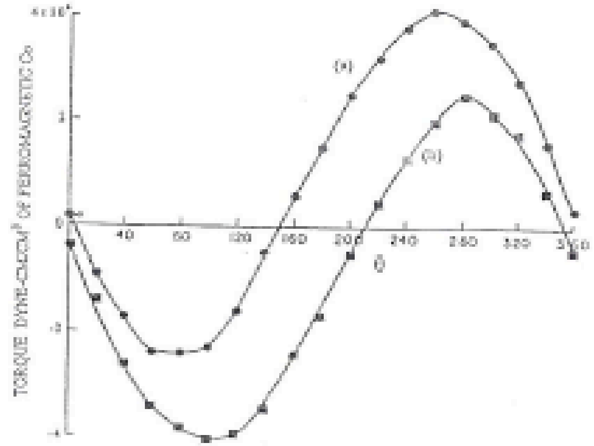

Rotational hysteresis of the same particles

Shifted hysteresis loop of Co particles measured on field cooling in 1 T to 77 K

Exchange bias of thin films

Néel 1964

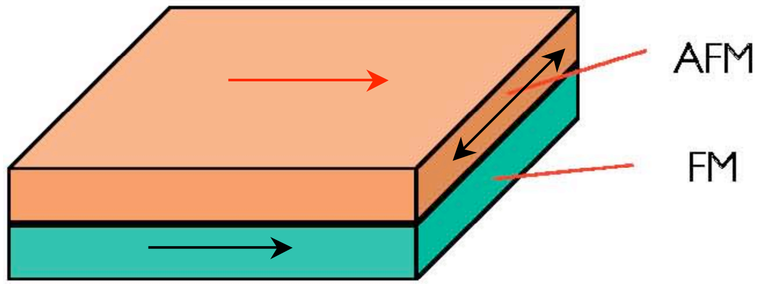

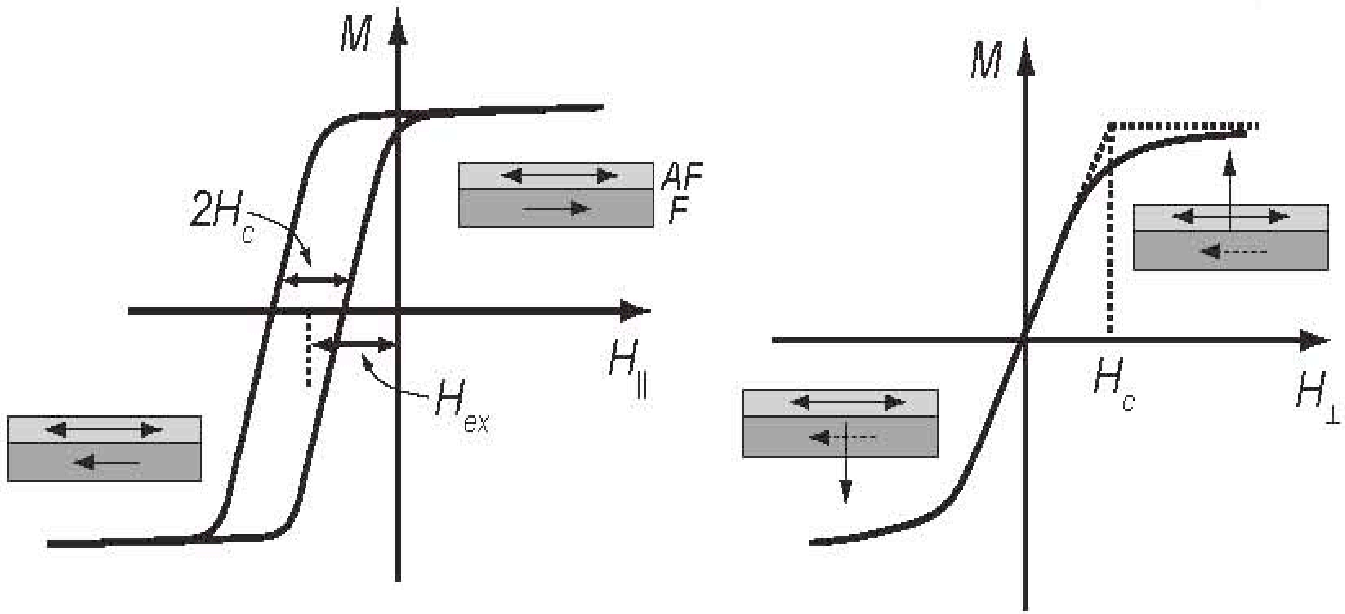

The effect of exchange bias on the hysteresis loop of a ferromagnetic layer coupled to an antiferromagnetic layer. The red arrow in the AF-layer shows the direction of the exchange field, which need not coincide with the antiferromagnetic axis. The loop on the left is measured with the applied field in this direction; the one on the right with the applied field in the perpendicular direction.

It is as if an effective field $H_{eff} = H + H_{ex}$ is acting on the film; $H_{ex} \approx 4$ kA/m; $\mu_0 H_{ex} \approx 50$ mT

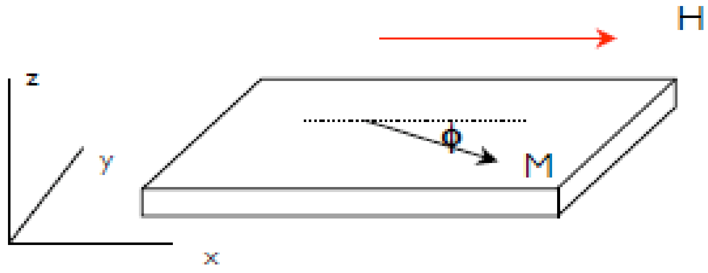

$$E_x = -\mu_0 M_p H_x \cos\phi - K_{ex}\cos\phi$$

$H_{ex} = K_{ex}/\mu_0 M^2$

$$E_y = -\mu_0 M_P H_y \cos(\pi/2 - \phi) - K_{ex}\cos\phi + K_u \sin^2\phi$$

The energies are better written per unit area of film as exchange bias scales with the area.

$K_{ex} = \sigma/t_p$ The energy per unit area is:

$$E_{\mathcal{A}} = -\mu_0 M_p H t_p \cos\phi - \sigma\cos\phi + K_u t_p \sin^2\phi$$

The corresponding field is $E_A/\mu_0 M_p t_p$

Minimize E_A $$\sin\phi[\cos\phi + (\sigma/2K_u t_p) + (M_p H/2K_u)] = 0$$

Switching occurs when $\phi=\pi/2$; $H = H_{ex} = -\sigma/M_p t_p$ Perpendicular anisotropy field $H_a = (\sigma+2K_u t_p)/\mu_0 M_p t_p$

Dependence on layer thickness

There is a threshold t_{af} necessary for exchange bias to become effective; $t_{crit}K_{as} \approx \sigma$;
t_{crot} = 10 nm, K_{af} = 20 kJ m^{-3} $\sigma \approx 0.2$ mJ m^{-2}

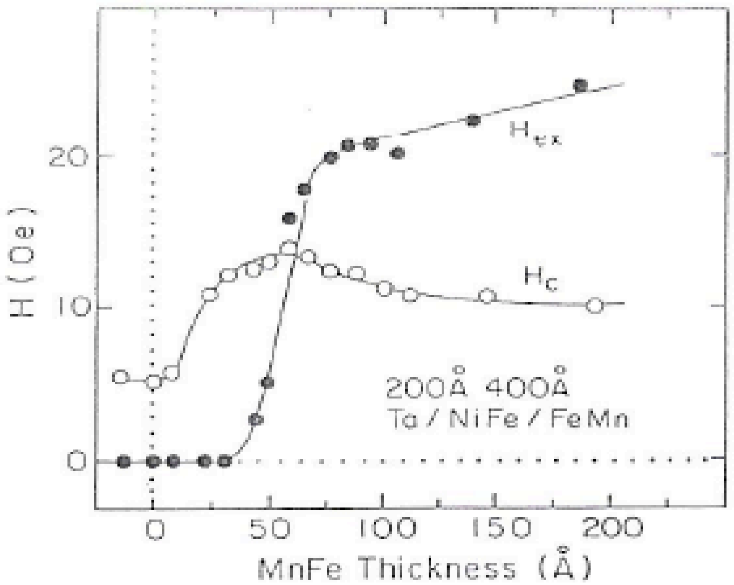

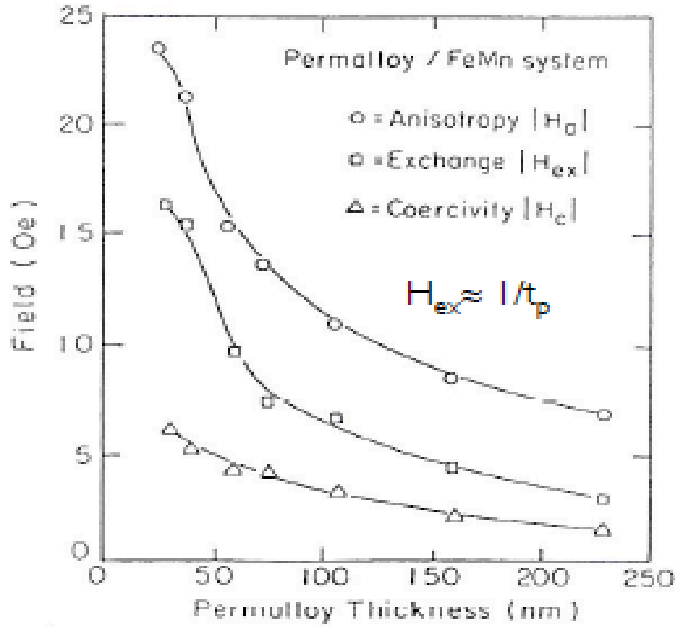

Fig 8.14 The dependence of exchange bias on the thickness of the antiferromagnetic layer (left) and on the thickness of the ferromagnetic layer (right)

Table 8.2. Antiferromagnetic Materials for Exchange Bias

		T_N(K)	T_b(K)	σ(mJ m^{-2})
FeMn	fcc; four noncollinear sublarrices; S ‖ {111}	510	440	0.10
NiMn	fct; antiferromagnetic 002 planes, S ‖ a	1050#	≈700	0.27
PtMn	fct; antiferromagnetic 002 planes, S ‖ c	975	500	0.30
$RhMn_3$	triangular spin structure	850	520	0.19
$Ir_{22}Mn_{78}$	fct; parallel spins in 002 planes, S ‖ c	690	540	0.19
$Pd_{52}Pt_{18}Mn_{50}$	fct; antiferromagnetic 002 planes	870	580	0.17
$aTb_{25}Co_{75}$*	$T_{comp} = 340$ K	600	>520	0.33
NiO	parallel spins in 111 planes, S ⊥<111>.	525	460	0.06
αFe_2O_3	canted antiferro-magnet, S ⊥c.	960		0.05

#Order-disorder transition

*Sperimagnetic; T_N is the Curie temperature.

T_b an irreversible tranition.

Exchange bias only becomes effective below a blocking temperature T_b which is considerably lower than T_N

Models for exchange bias

*Atomically flat antiferomagnetic surface.

A) could be spin compensated; $\sigma = 0$; B) could present one ferromagnetic plane; $\sigma = A/d \approx 200$ mJ m^{-2}

*Only about 1/1000 of the spins seem to participate in the exchange coupling.

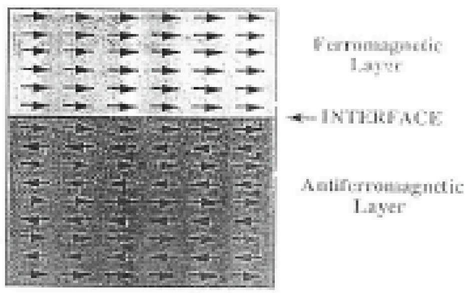

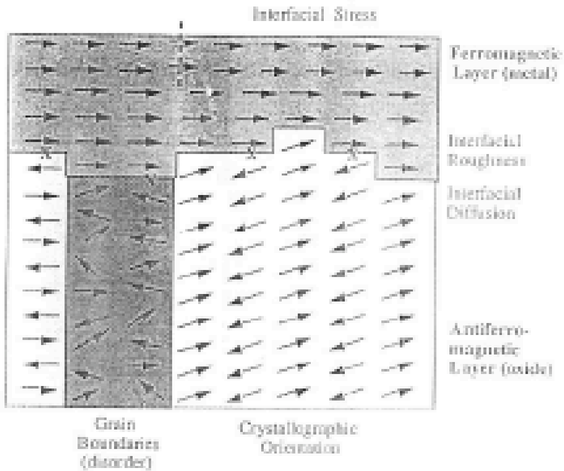

Surface is inevitably rough. Regions of dimension L contain $(L/a)^2$ atoms. Uncompensated moment is that of $\sqrt{(L/a)^2}$ atoms. Hence L $\approx$ 1000a $\approx$ 200 nm. OK But these regions will themselves add randomly.

* Exchange bias may arise from defects of grain boundaries where there are frustrated spins

Models for exchange bias

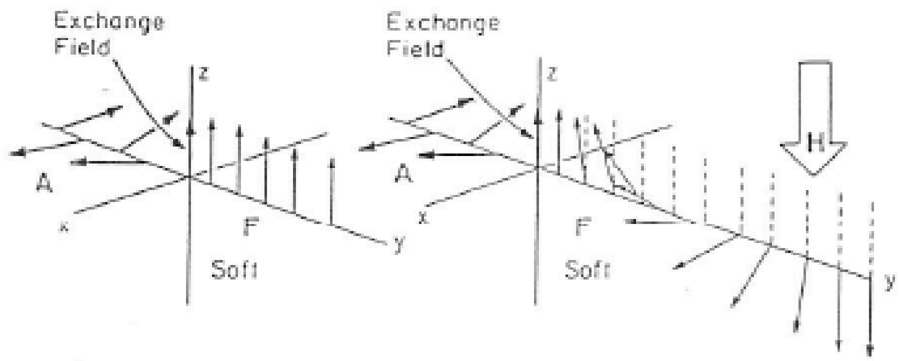

Fig 8.16 Formation of a domain wall at an interface of a soft ferromagnetic layer exchange-coupled to an antiferromagnet.

* Interfacial coupling leads to perpendicular fm and afm axes. Coupling energy will be similar to that in a 90 degree domain wall; $(1/2)\sqrt{(KA_{af})} \approx 0.4$ mJ m^{-2}

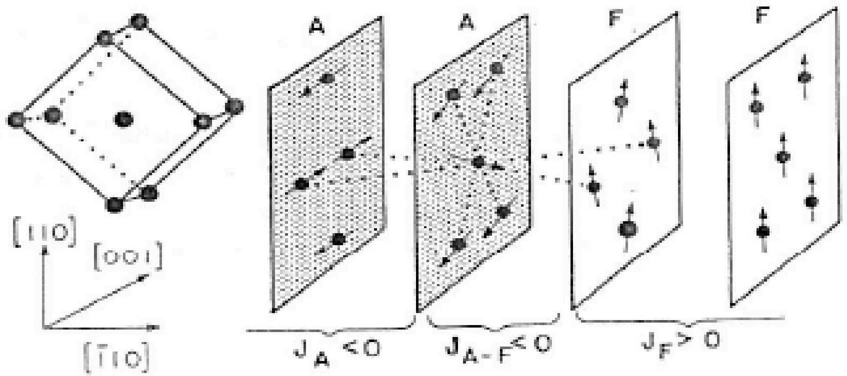

Fig. 8. 17 . An explanation of how the ferromagnetic and antiferromagnetic axes may couple perpendicular. There is a common [110] plane with antiferromagnetic coupling across it.

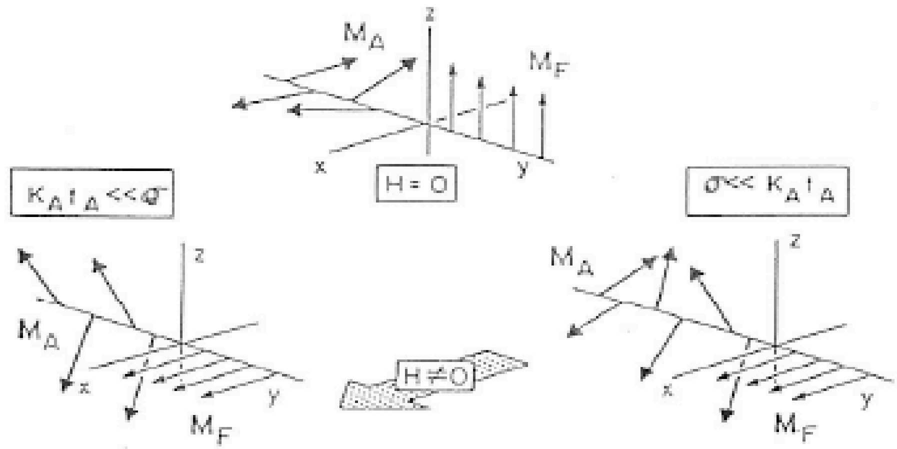

Fig. 8. 18 . The interfacial magnetic configuration showing a spin flop in the antiferromagnet when the anisotropy of the antiferromagnet is small.

Exchange biased GMR spin valve

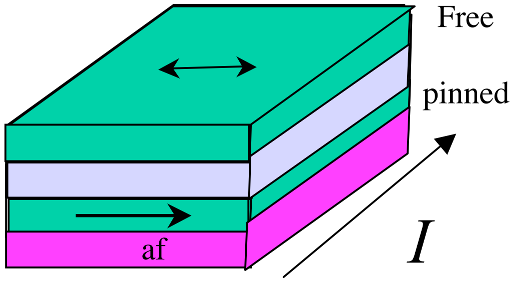

GMR spin valve

Exchange-biased stack

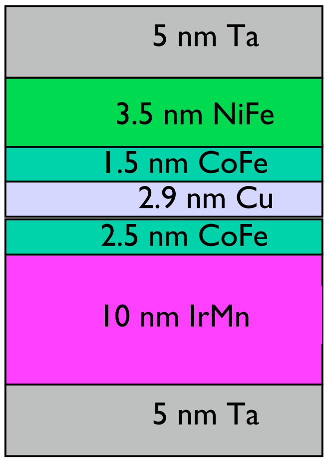

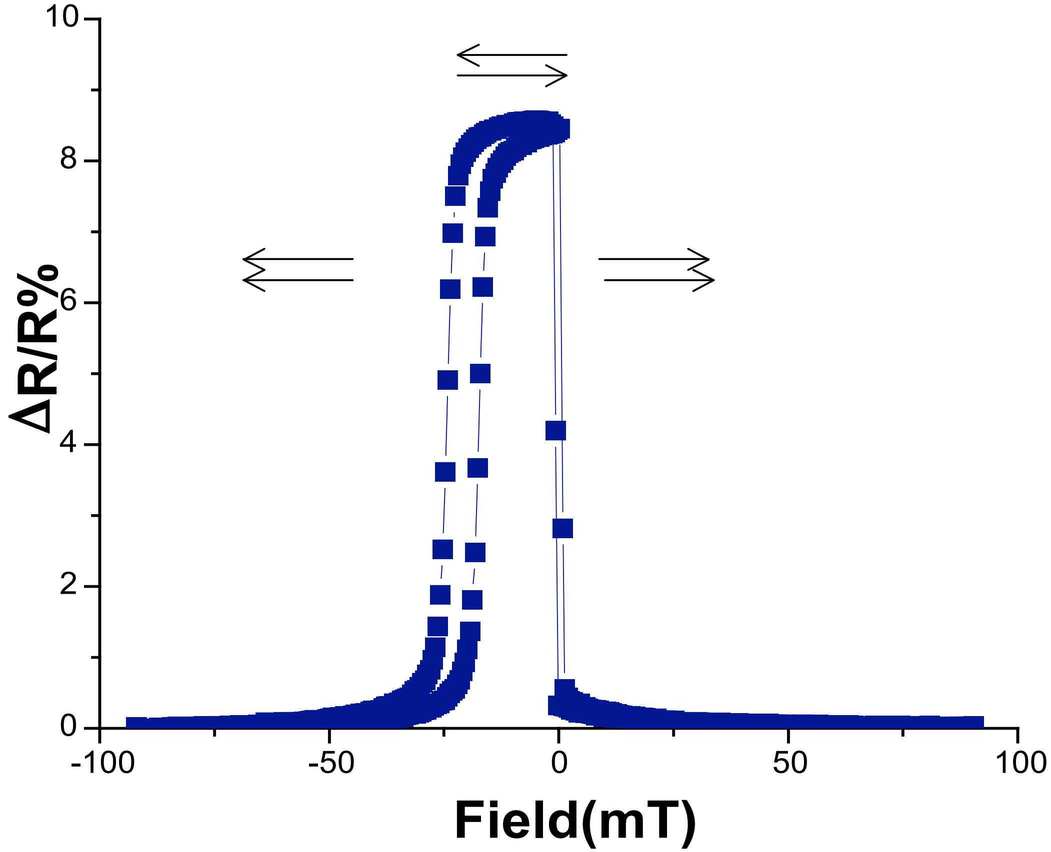

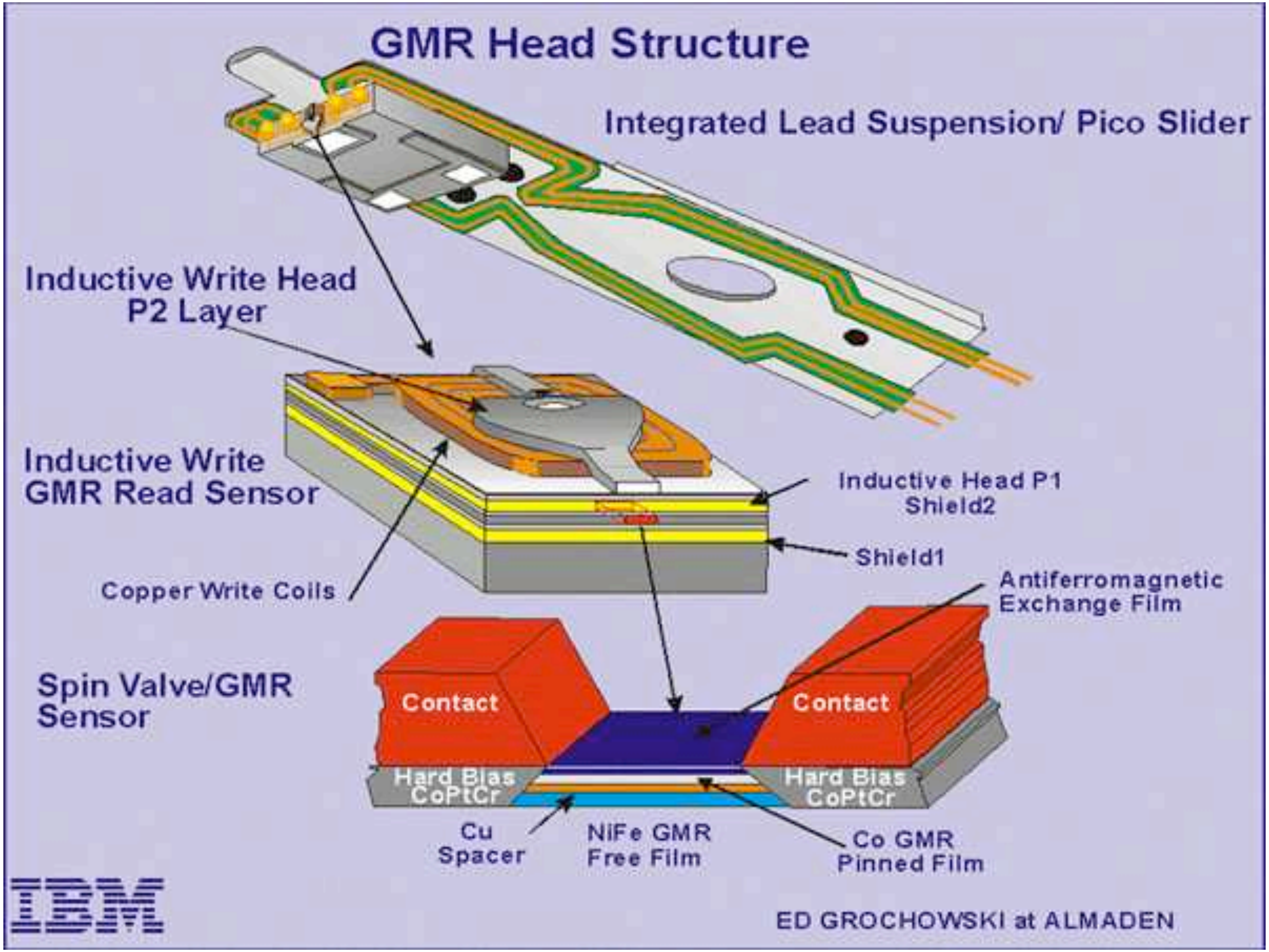
GMR Head Structure
Integrated Lead Suspension/ Pico Slider
Inductive Write Head
P2 Layer
Inductive Write
GMR Read Sensor
Inductive Head P1
Shield2
Shield1
Copper Write Coils
Antiferromagnetic
Exchange Film
Spin Valve/GMR
Sensor
Contact
Contact
Hard Bias
CoPtCr
Hard Bias
CoPtCr
Cu
Spacer
NiFe GMR
Free Film
Co GMR
Pinned Film
IBM
ED GROCHOWSKI at ALMADEN

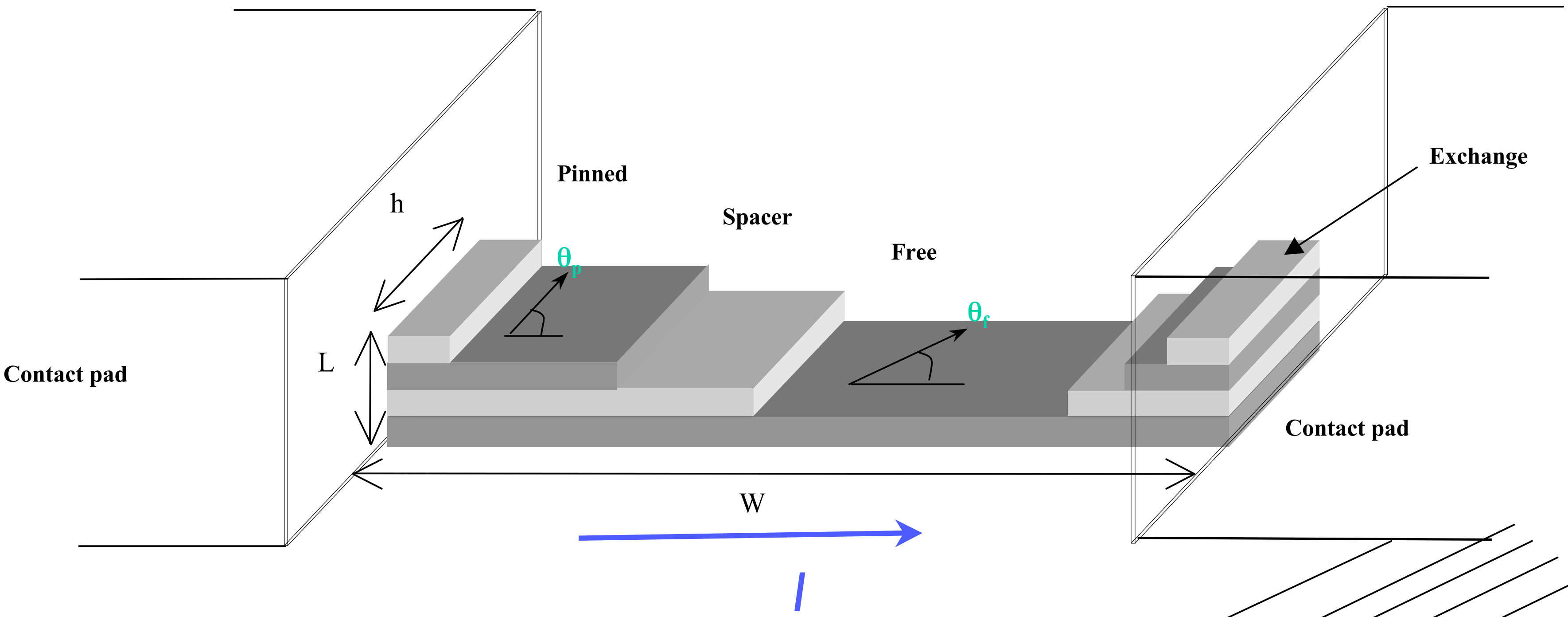

$$\Delta V = (1/2)\, IR\, (\Delta R/R)\langle 1 - \cos(\theta_p - \theta_f)\rangle$$

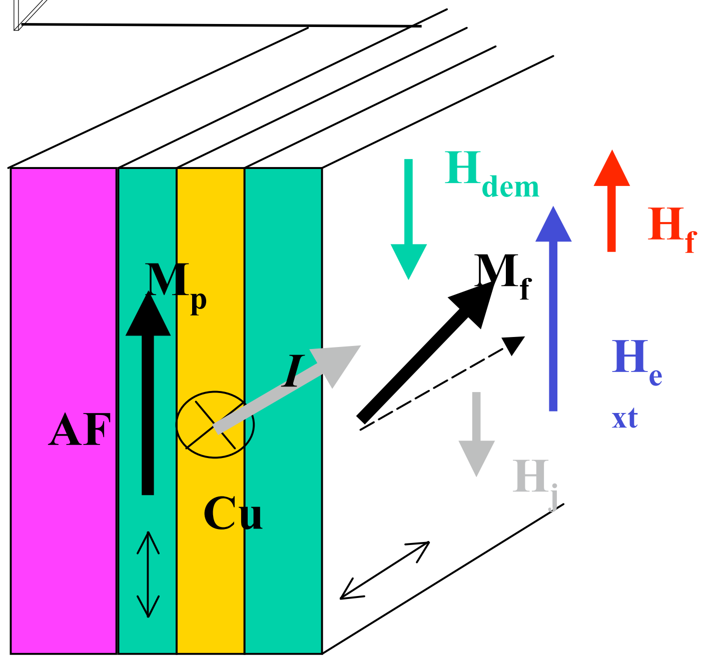

4.1 Spin valve sensors

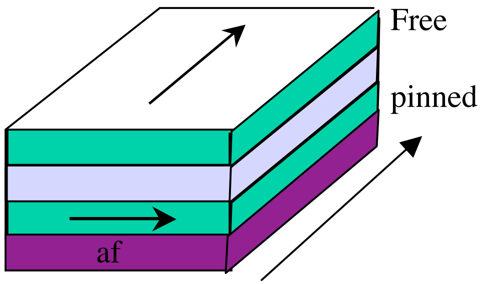

For maximum sensitivity, the free layer should lie with its magnetization perpendicular to the pinned layer.

This can be done using shape anisotropy, or with a magnetic stray field created by permanent magnet elements.

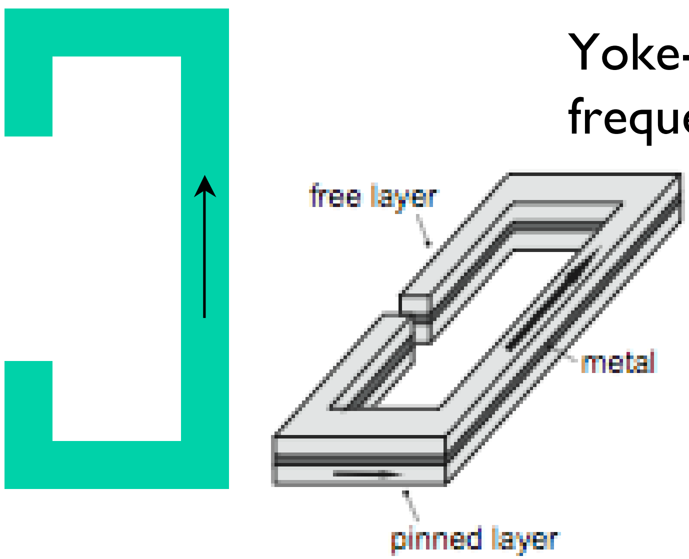

Yoke-type sensor. Combined with flux concentration and frequency modulation, the sensitvity of spin valve sensors approaches that of a SQUID.

Transfer curve of GMR spin valve

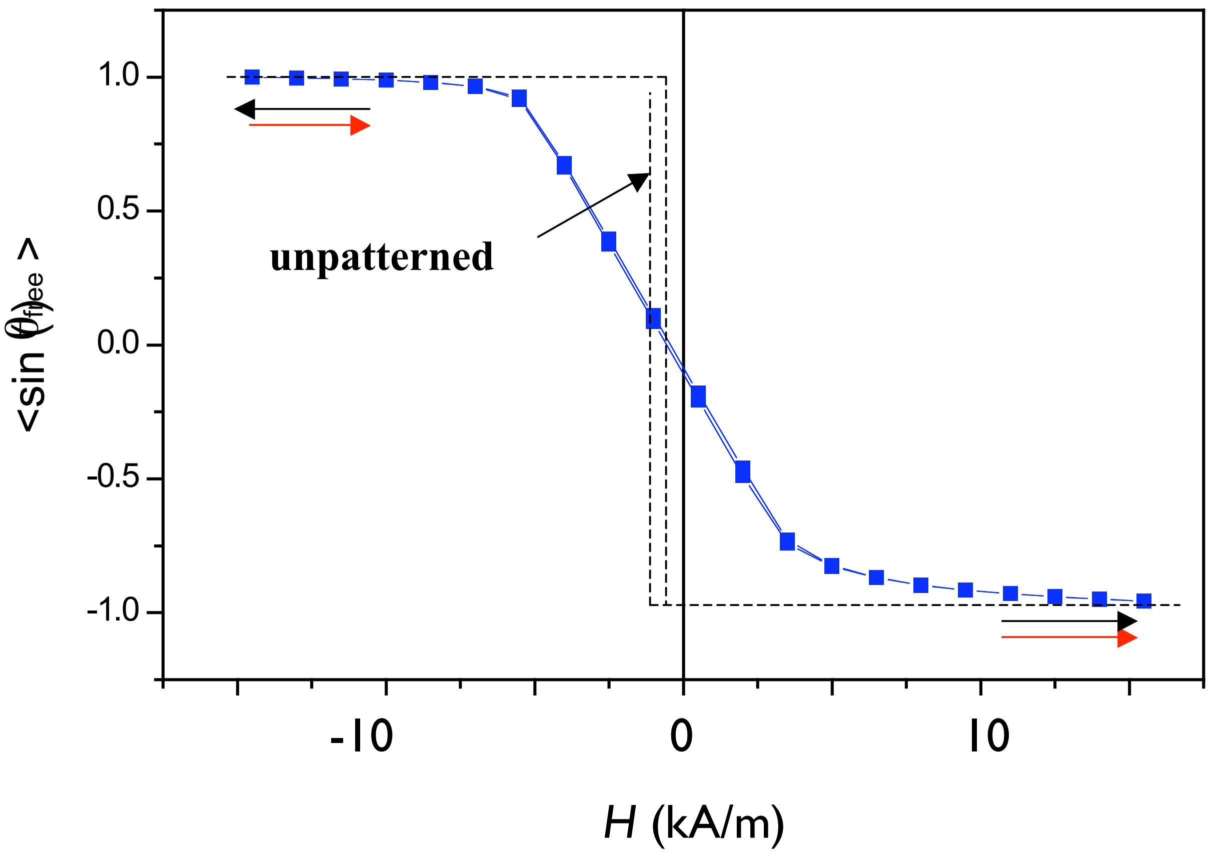

Some GMR spin valve stacks

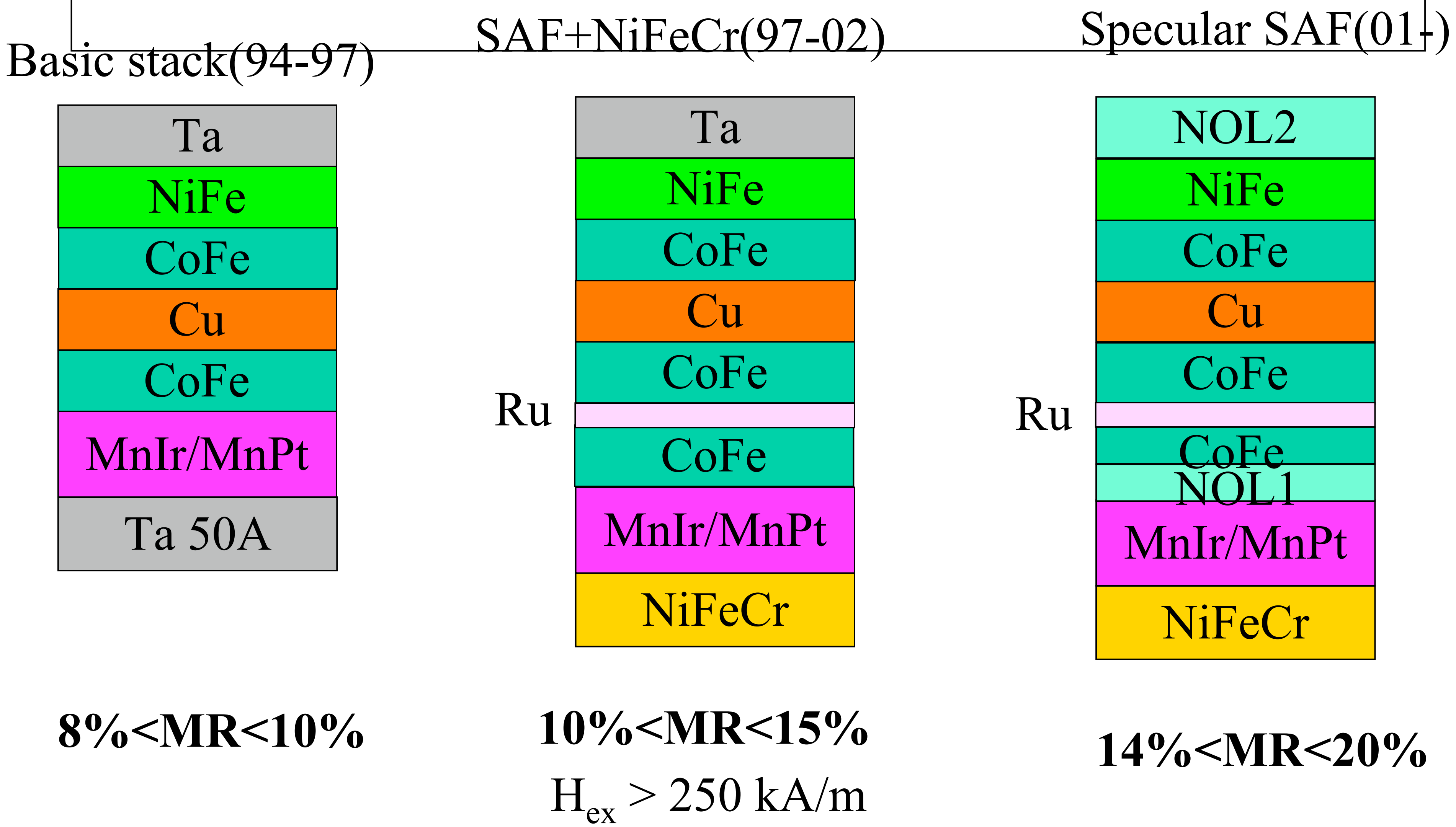

3.2 Indirect exchange coupling

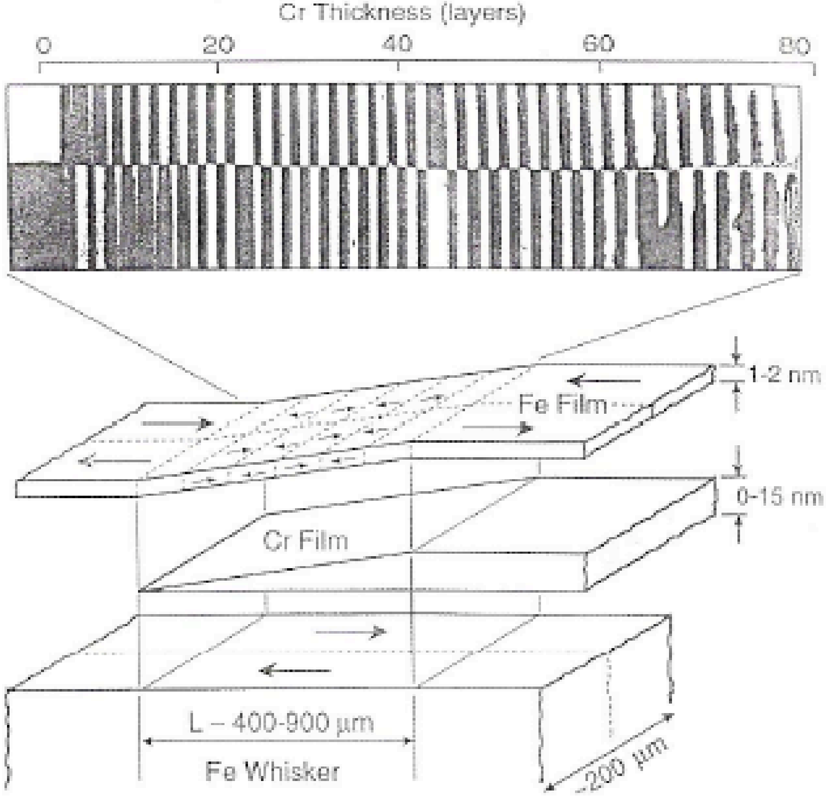

Fig. 8. 17 An experiment which demonstrates the oscillating spin polarization as a function of spacer thickness.

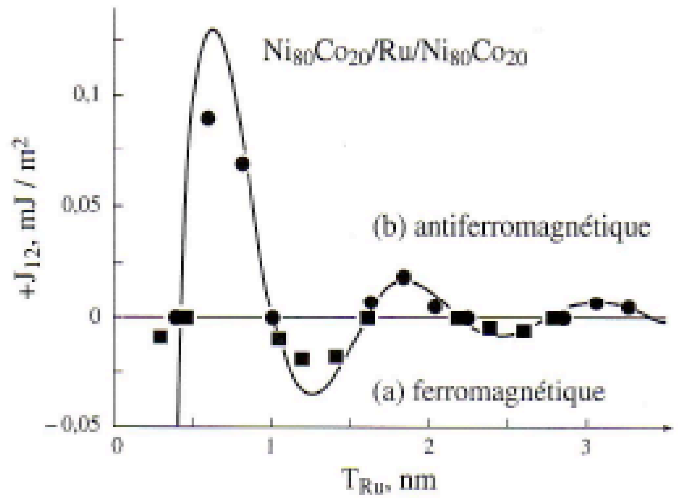

Fig 8.21 Oscillations of the exchange coupling between ferromagnetic layers as a function of the ruthenium spacer thickness

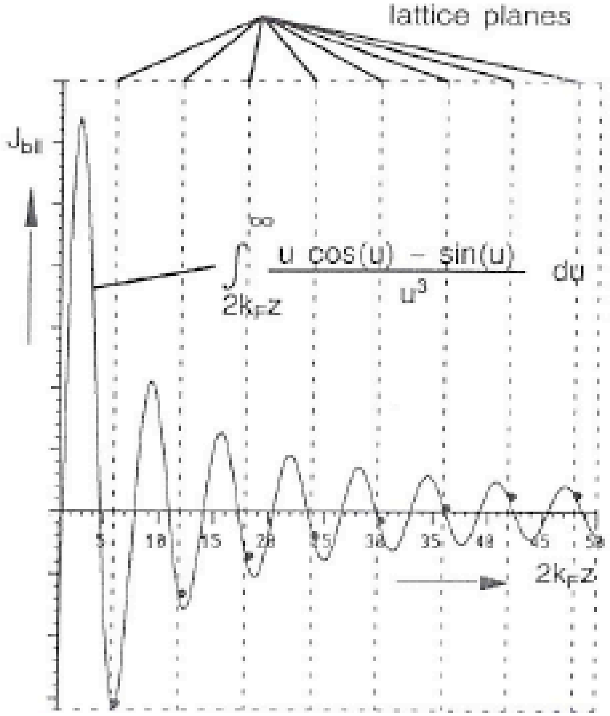

Fig 8.20 The aliasing effect

Best for af coupling is 0.8 nm Ru

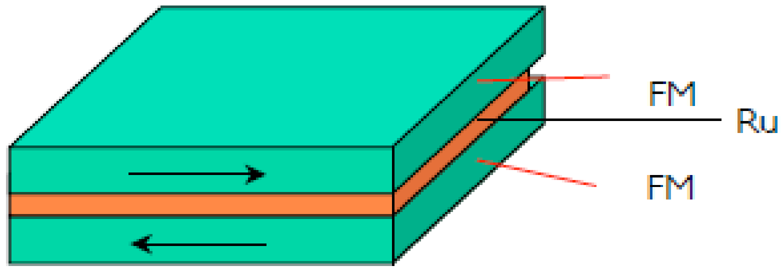

Artificial Antiferromagnet (SAF)

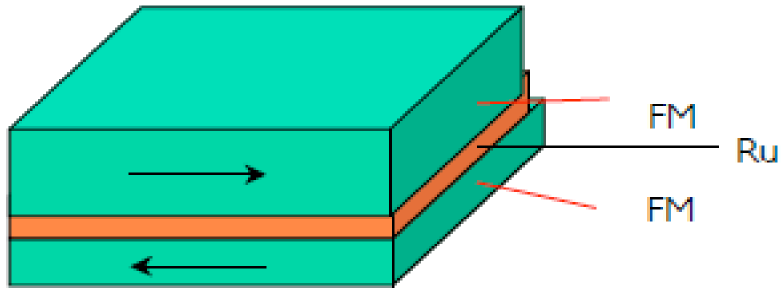

Artificial Ferrimagnet

Table 8.3. Antiferromagnetic interlayer exchange coupling in multilayers

		t_s(nm)	σ_{ex}(mJ m^{-2})
Fe	Cu	1.0	−0.3
Fe	Cr	0.9	−0.6
Co	Cu	0.9	−0.4
Co	Ag	0.9	−0.2
Co	Ru	0.7	−5.0
$Ni_{80}Fe_{20}$	Ag	1.1	−0.01

3.3 Dipolar coupling

Néel orange peel coupling

A perfectly smooth film creates no stray field. Correlated roughness leads to orange-peel coupling

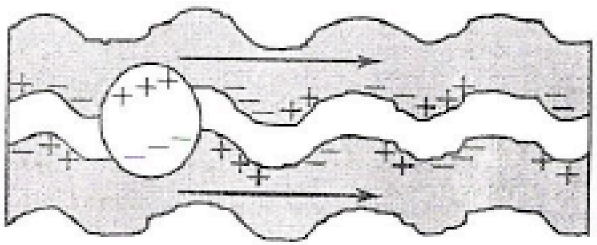

The orange-peel effect

$$\sigma_d = \frac{\pi^2}{\sqrt{2}} \frac{\delta_s^2}{l} \mu_0 M_s^2 \exp(-2\pi\sqrt{2}t_s/l)$$

With t_n,the spacer thickness - 5nm, roughness δ = 1 nm, period l = 20 nm, the coupling is 0.03 mJ m^{-2}

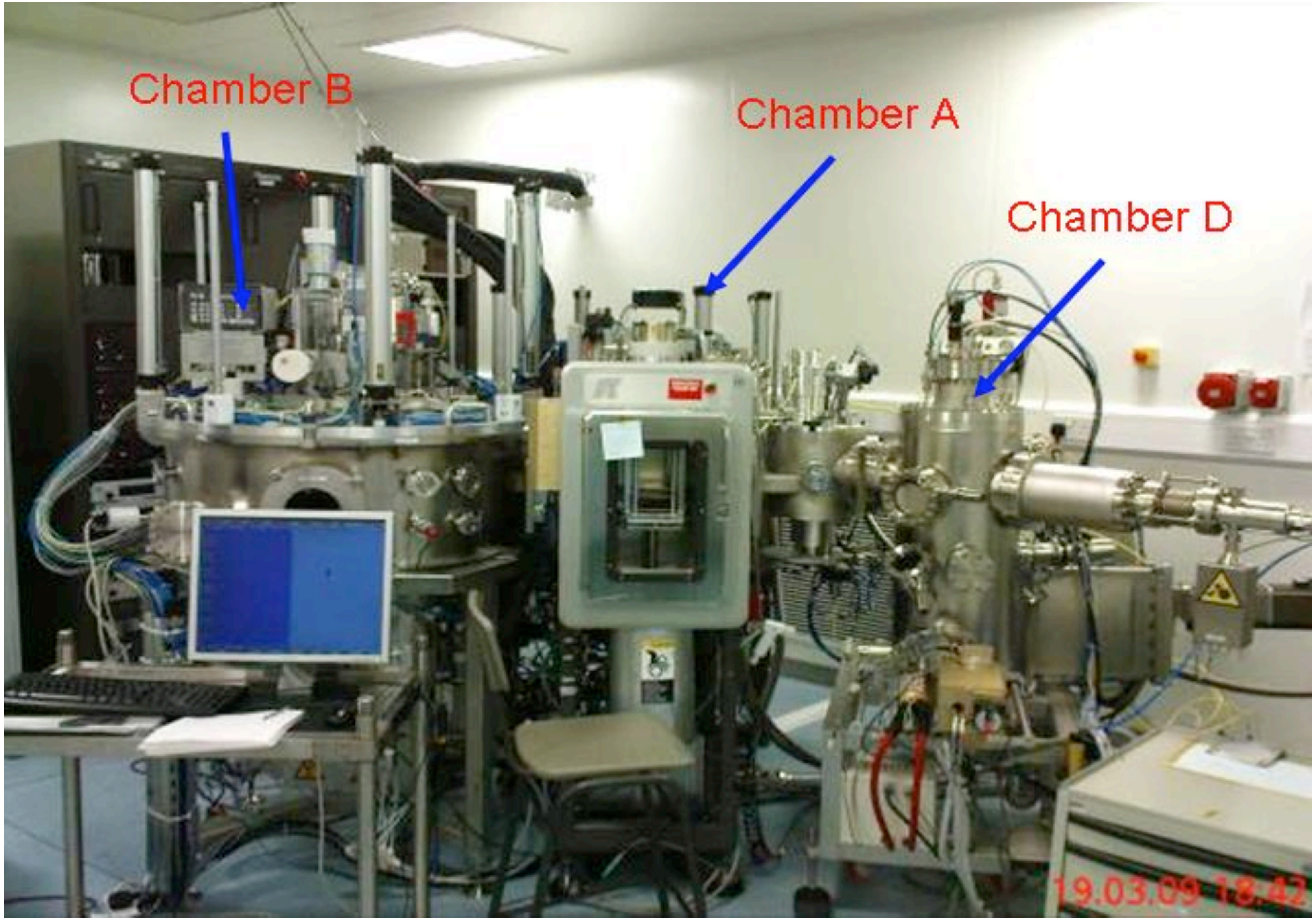

Chamber A: Metal Sputtering (6 guns + 1 ion gun)
Chamber B: Oxide Sputtering (8 guns + 1ion gun)
Chamber C: UHV E-beam (4 pockets) + Sputtering (1 gun)

The Shamrock sputtering tool

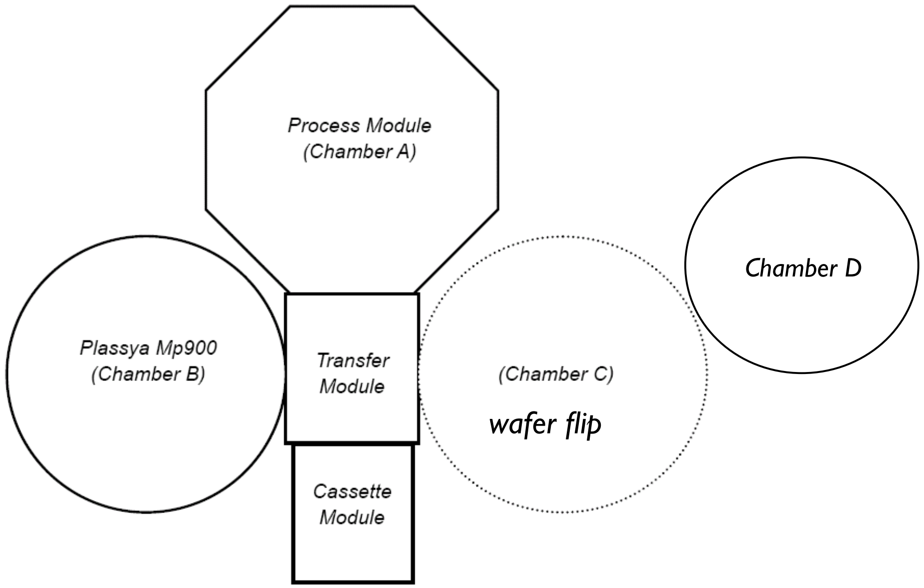

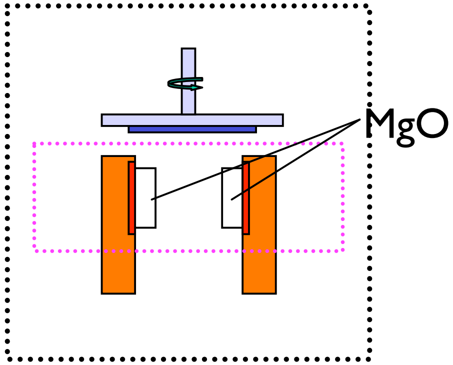

- **Chamber B**

Base pressure < 3 x 10⁻⁶ Pa

2 Target Facing Target guns (MgO)

2 Three-target custers.

- **Chamber A**

Base pressure < 10⁻⁵ Pa

6 Series-III S Guns (DC& RF)

- **Chamber D**

Base pressure < 10⁻⁷ Pa

e-beam evaporation

1 Sputtering source

Sputtering

The most widely used method in thin-film growth. Reproducible, stable.
Involves non-thermal transport based on momentum transfer from energetic ions, usually Ar^+ (mixed with G_2 or N_2 for reactive sputering

DC sputtering is used for metals. Target potential ≈ 200 V

Source-substrate distance ≈ 10 cm.

P ~ 0.05 - 1 Pa so the sputtered atoms undergo a few commissions before reaching the substrate.

Efficiency is improved using a magnetron cathods. Permanent magnets create a magnetic field at the target surface which causes the electrons to follow helical trajectories which increase the ionization efficiency.

Deposition rates are up to 10 nm s^{-1}

Best control by ion beam deposition

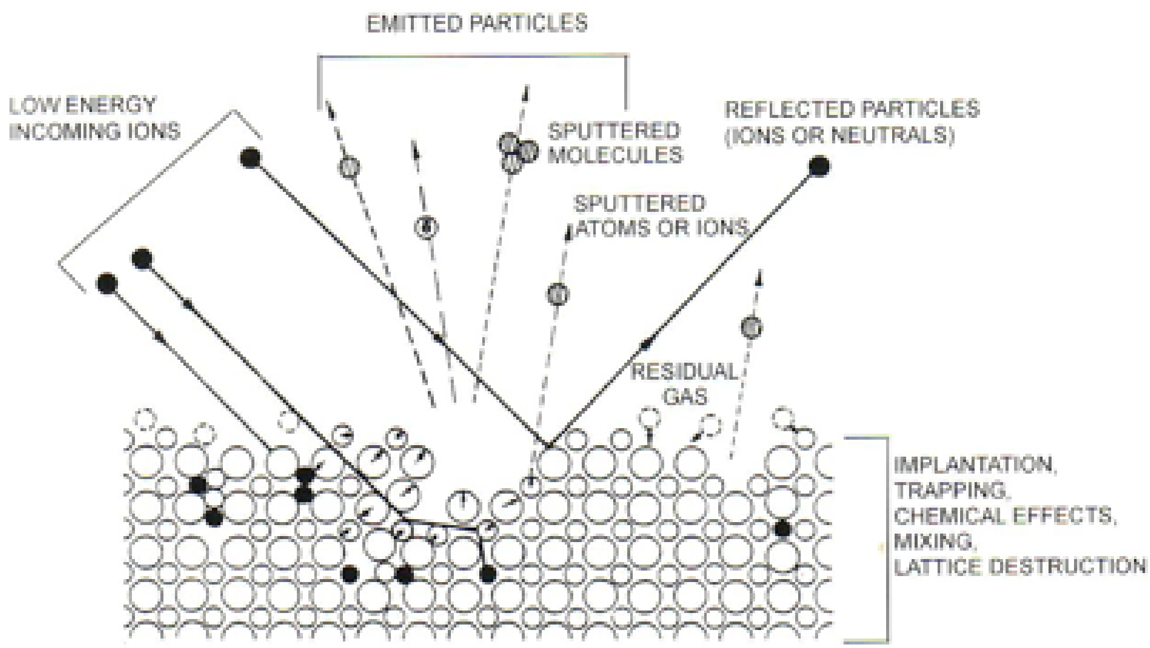

General ion-surface interaction processes

RF sputtering is used for insulators

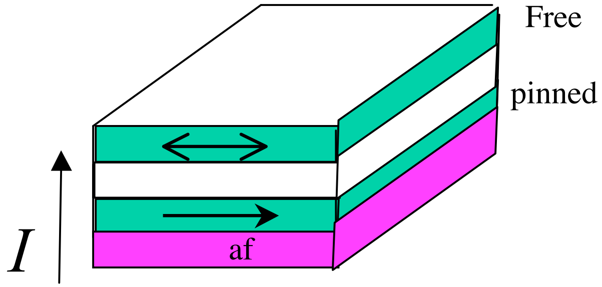

TMR spin valve

Exchange-biased stack

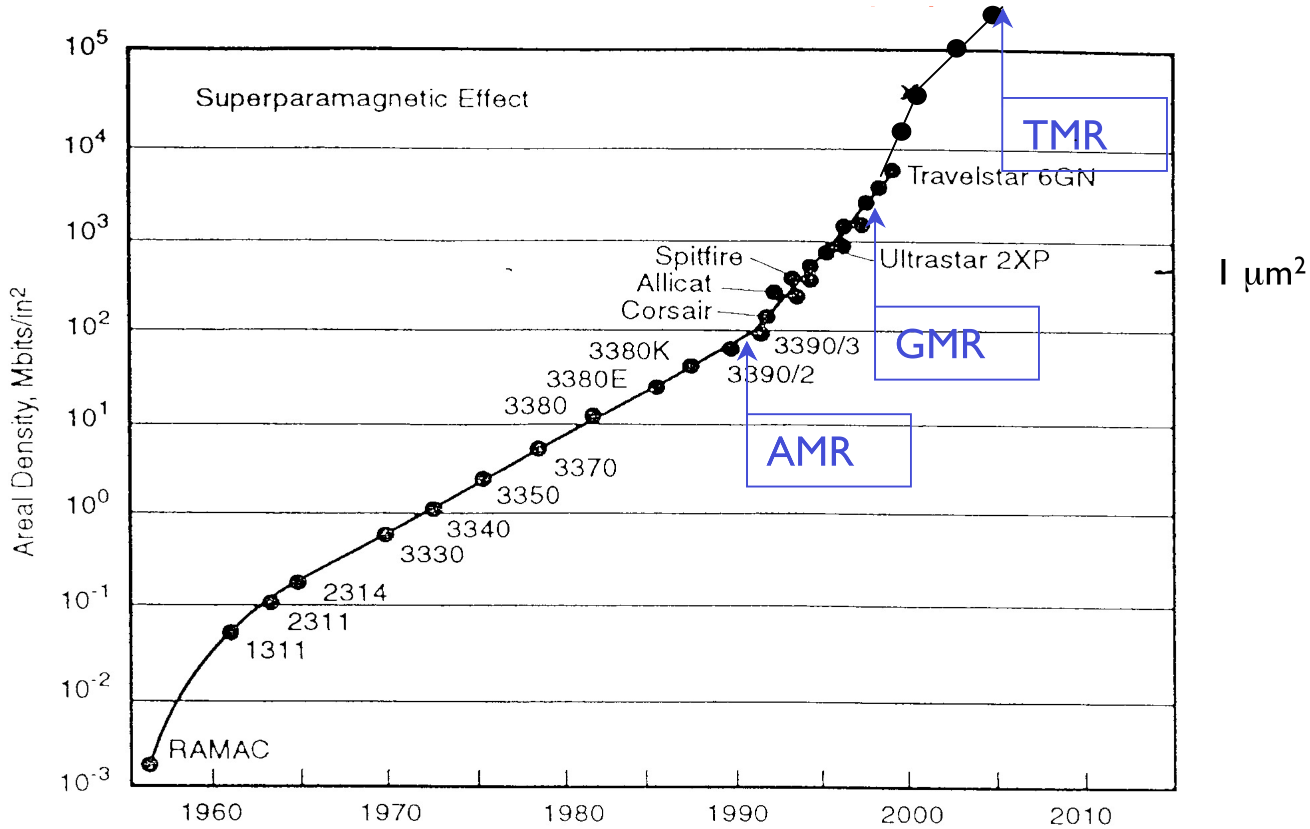

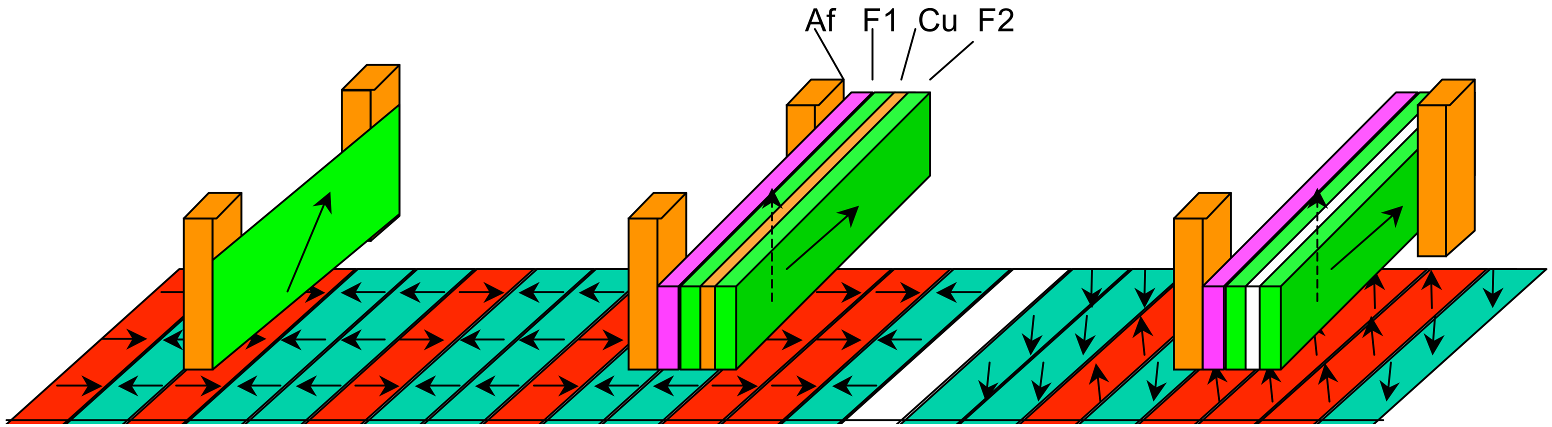

AMR GMR TMR

Tunnel magnetoresistance (TMR)

$$\boxed{MR = (R_{\uparrow\downarrow} - R_{\uparrow\uparrow})/R_{\uparrow\uparrow}}$$

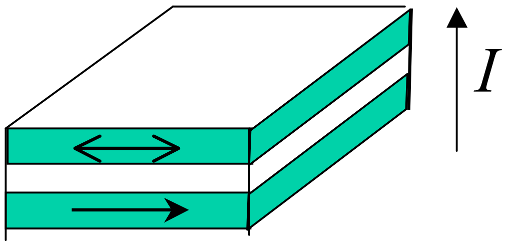

magnetic tunnel junction

Parallel

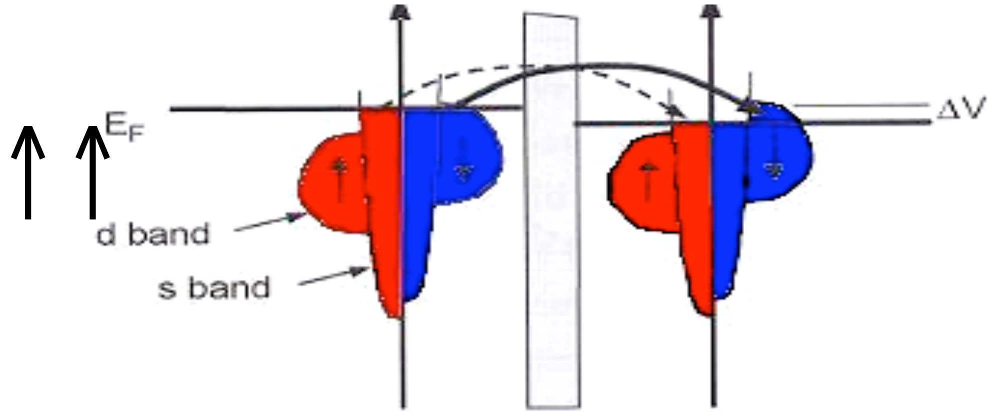

Antiparallel

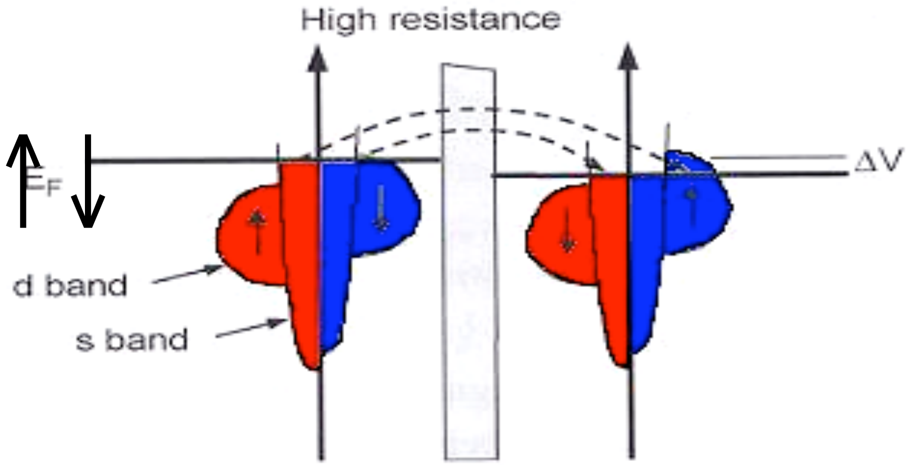

Julière formula:
$MR = 2P_1P_2/(1 - P_1P_2)$

If $P_1 = P_2$

$$\boxed{MR = 2P^2/(1 - P^2)}$$

Taking P = 45%, MR = 51%

3.6 Magnetic tunnel junctions

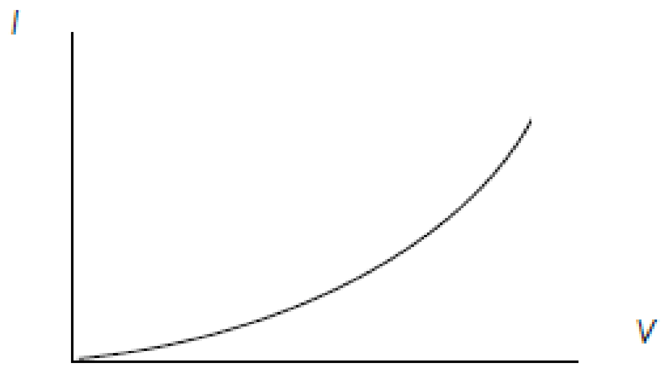

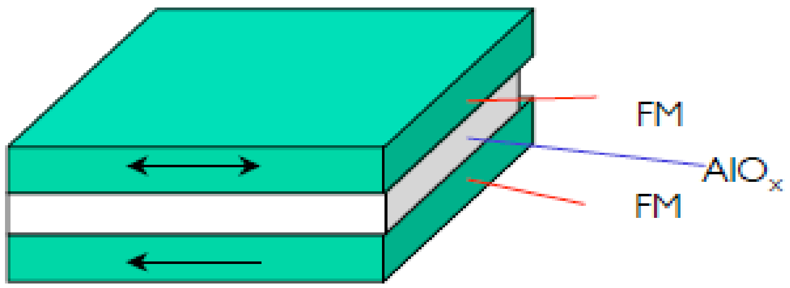

Magnetic tunnel junction

$\boxed{I = GV + \gamma V^3}$

$$G = (3e^2/2w\hbar^2)(2me\phi)^{1/2}\exp\{-(4\pi w/\hbar)(2me\phi)^{1/2}\}$$
$$\gamma = \pi m/3\phi(ew/\hbar)^2.$$

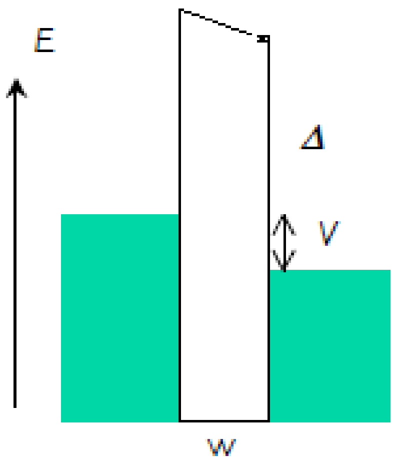

- Nonlinear I:V
- Current decreases exponentially with thickness w
- Little temperature dependence

Juliere formula for TMR

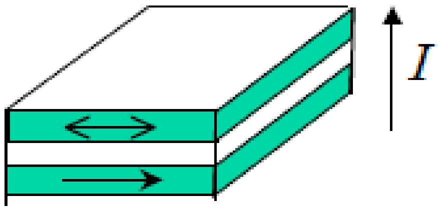

magnetic tunnel junction

$$G_p \propto N_{1\uparrow}N_{2\uparrow} + N_{1\downarrow}N_{2\downarrow}$$
$$G_{ap} \propto N_{1\uparrow}N_{2\downarrow} + N_{1\downarrow}N_{2\uparrow}$$

Parallel ↑ ↑

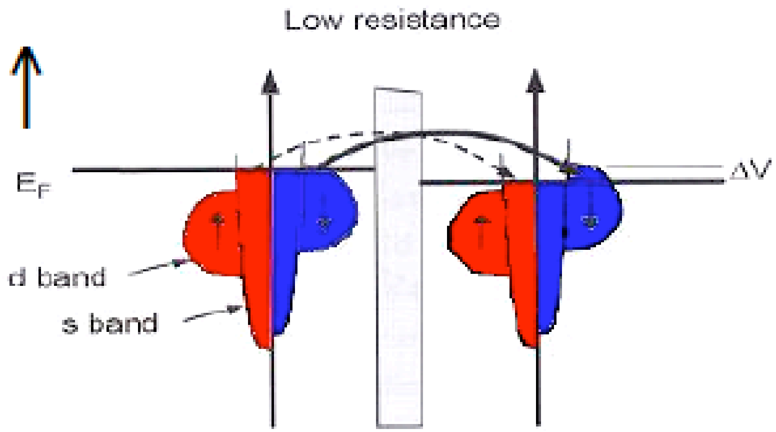

Antiparallel ↑ ↓

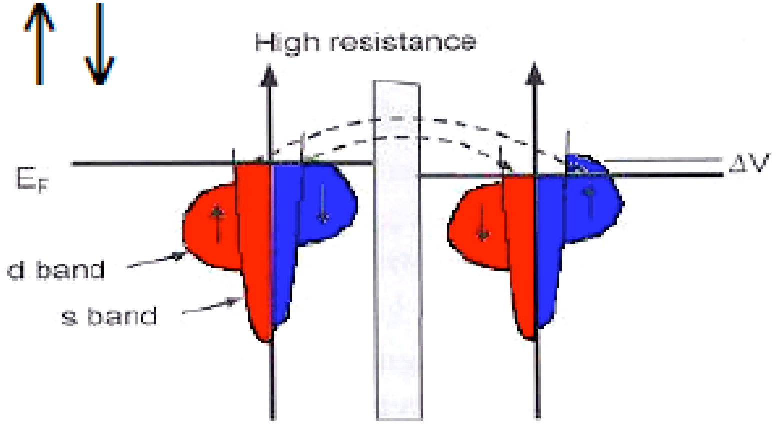

Jullière formula:
MR = $2P_1P_2/(1 - P_1P_2)$

If $P_1 = P_2$

$\boxed{\text{MR} = 2P^2/(1 - P^2)}$

Taking P = 45%, MR = 51%

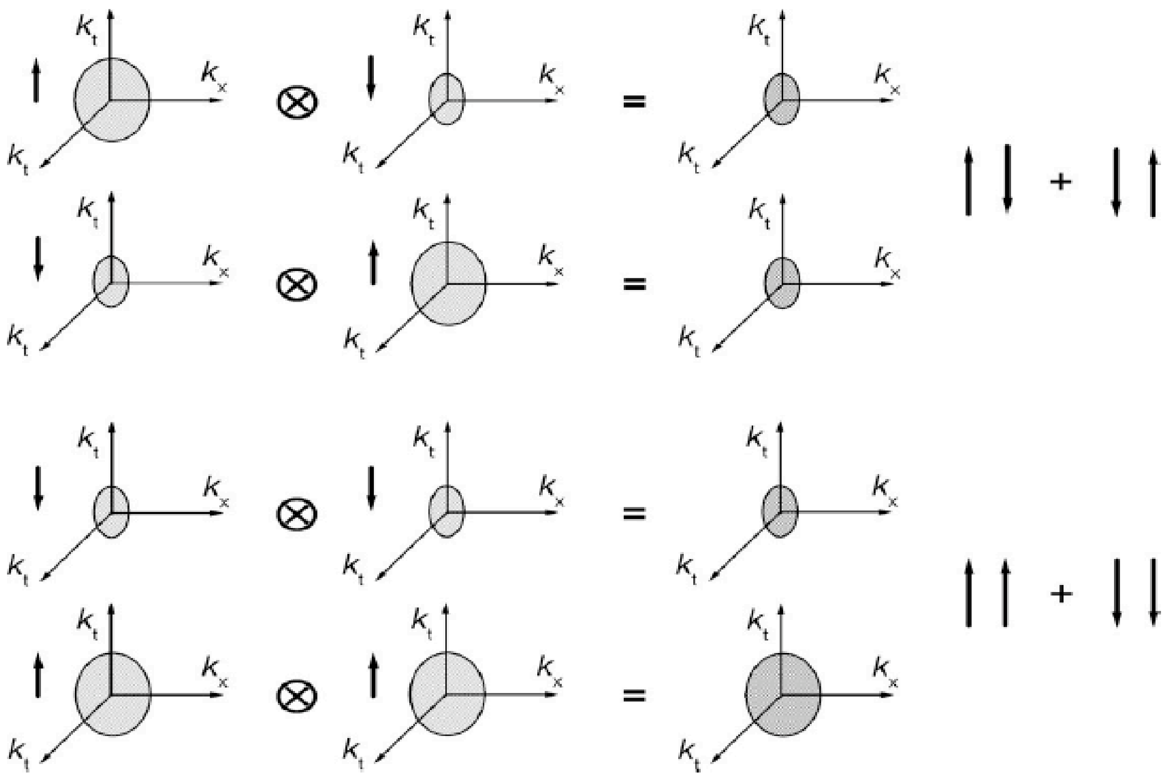

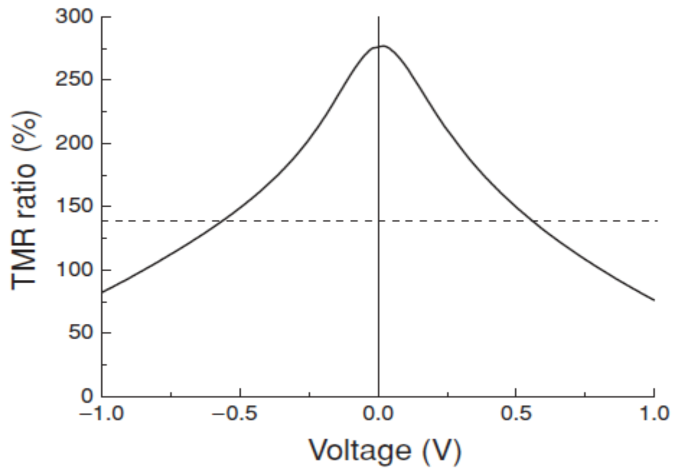

Bias-dependence of TMR

Resistance of a magnetic tunnel junction composed of a CoFe and a Co film separated by a thin layer of amorphous AlO_x. The device is a pseudo spin valve as the two layers have different coercivities, as shown by the AMR measurements in the top two panels. (J. S. Hoodera, L. R. Kinder, T.M. Wong *et al.*, *Phys. Rev. Letters*, **7**4, 3273 (1975).)

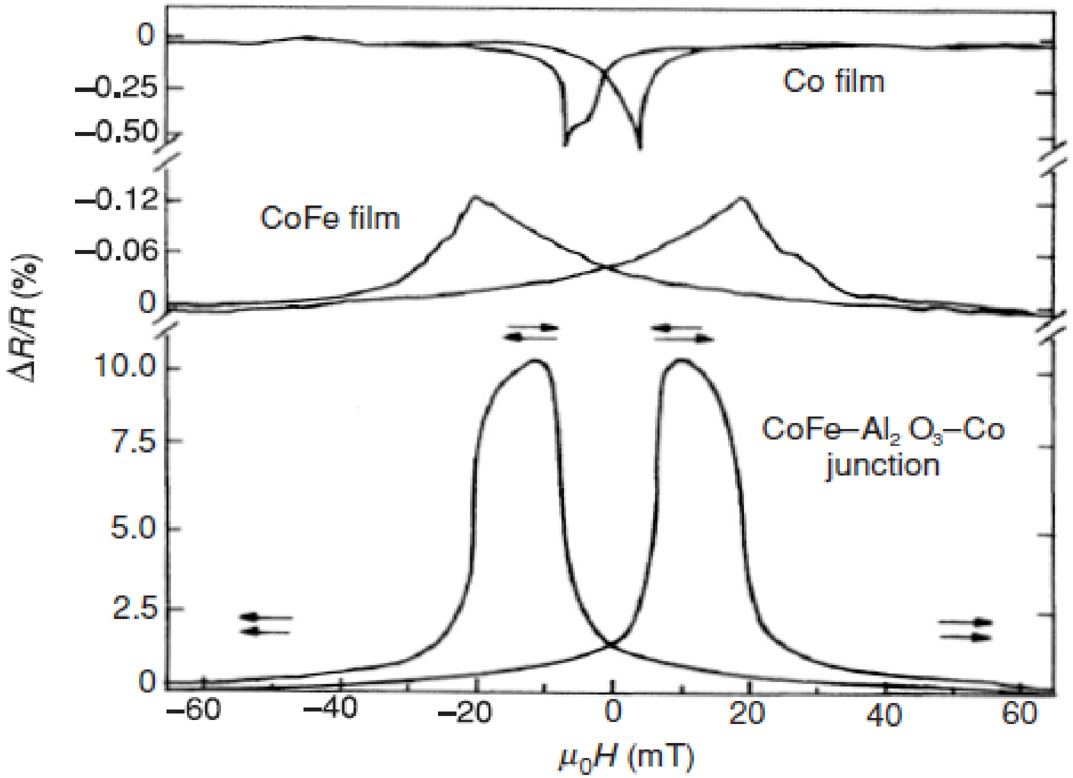

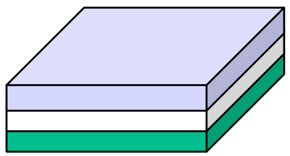

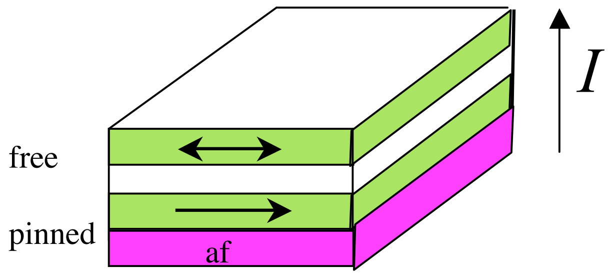

planar magnetic tunnel junction (MTJ)

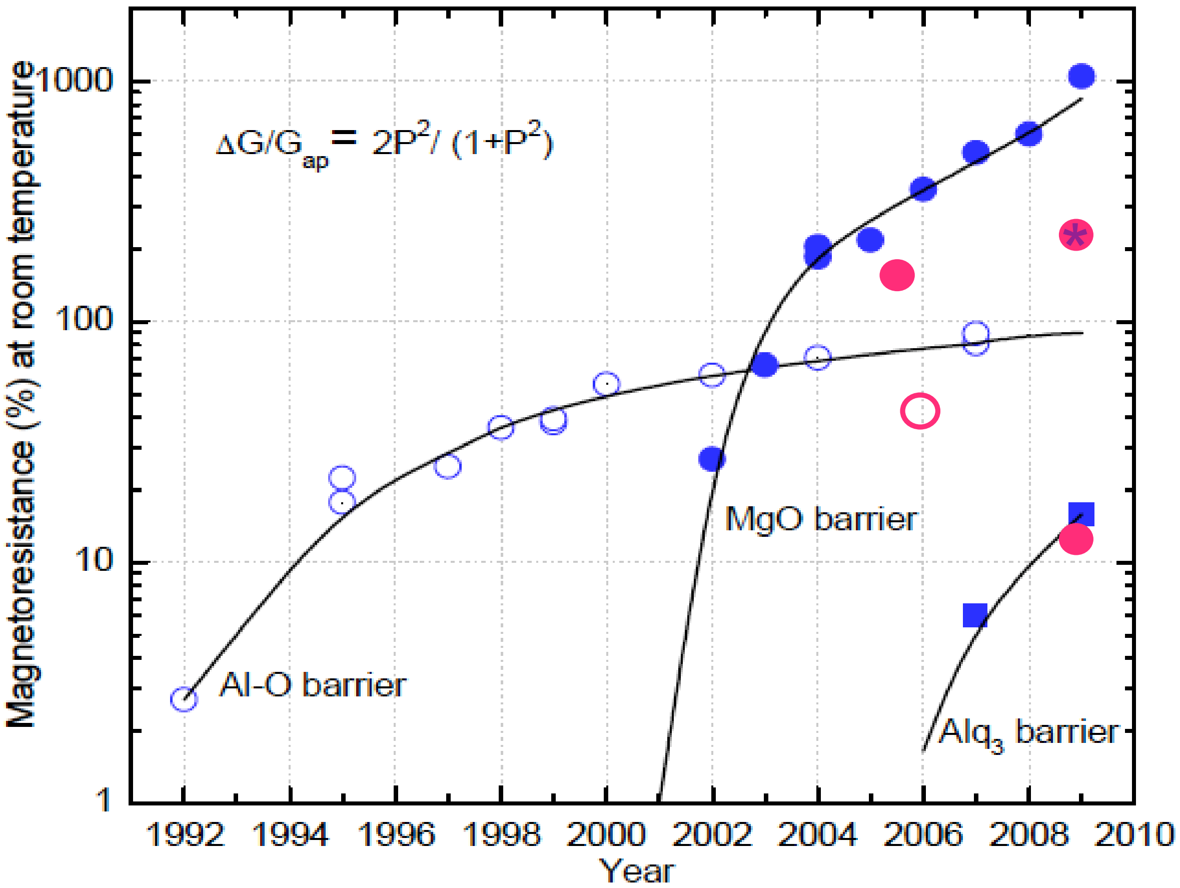

First-generation devices use a nanolayer of disordered aluminium oxide as the tunnel barrier, giving TMR of up to 70% (dark blue).

Crystalline MgO barriers improve the sensitivity by a factor of four (red),

SSP Parkin et al, *Nature Materials* **3**, 862 (2004). S. Yuasa *et al* , *Nature Materials* **3**, 866 (2004).

TMR > 200 %

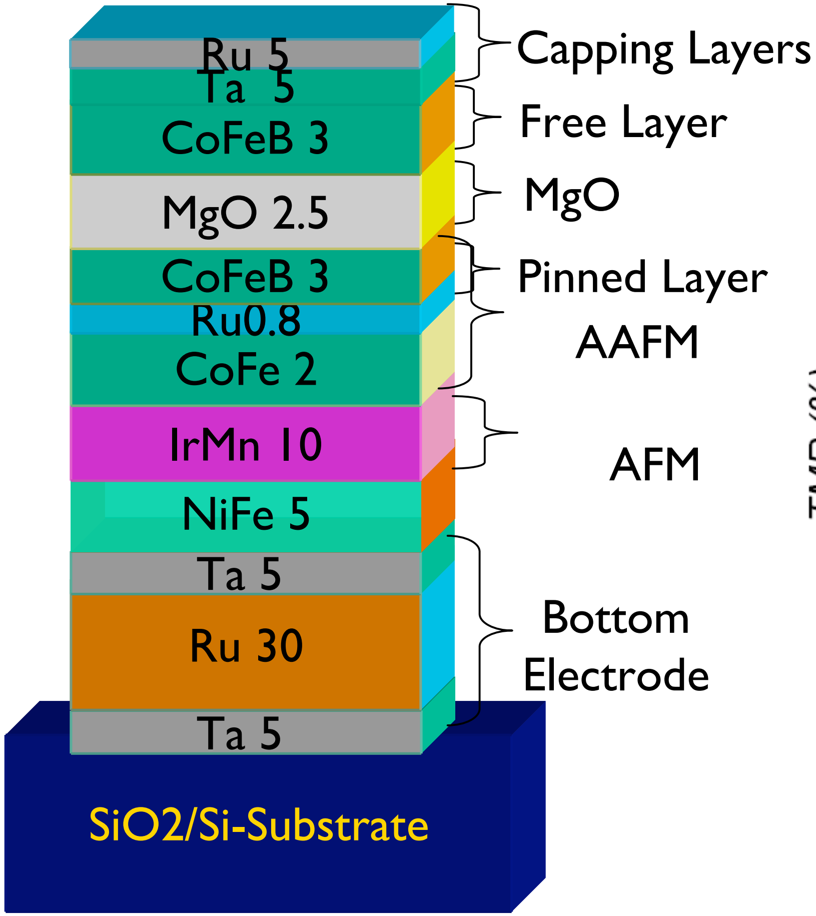

Magnetoresistance is > 100%, 10 times as great as for GMR spin valves

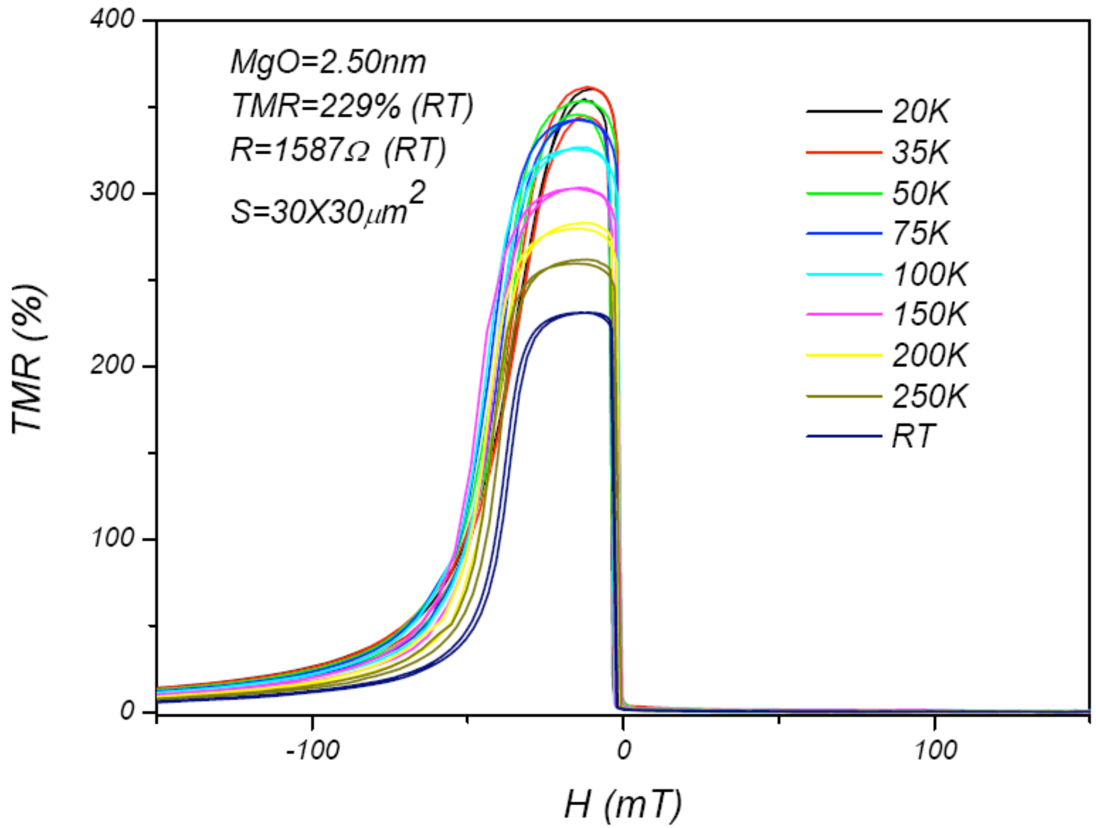

MgO barrier as spin filter

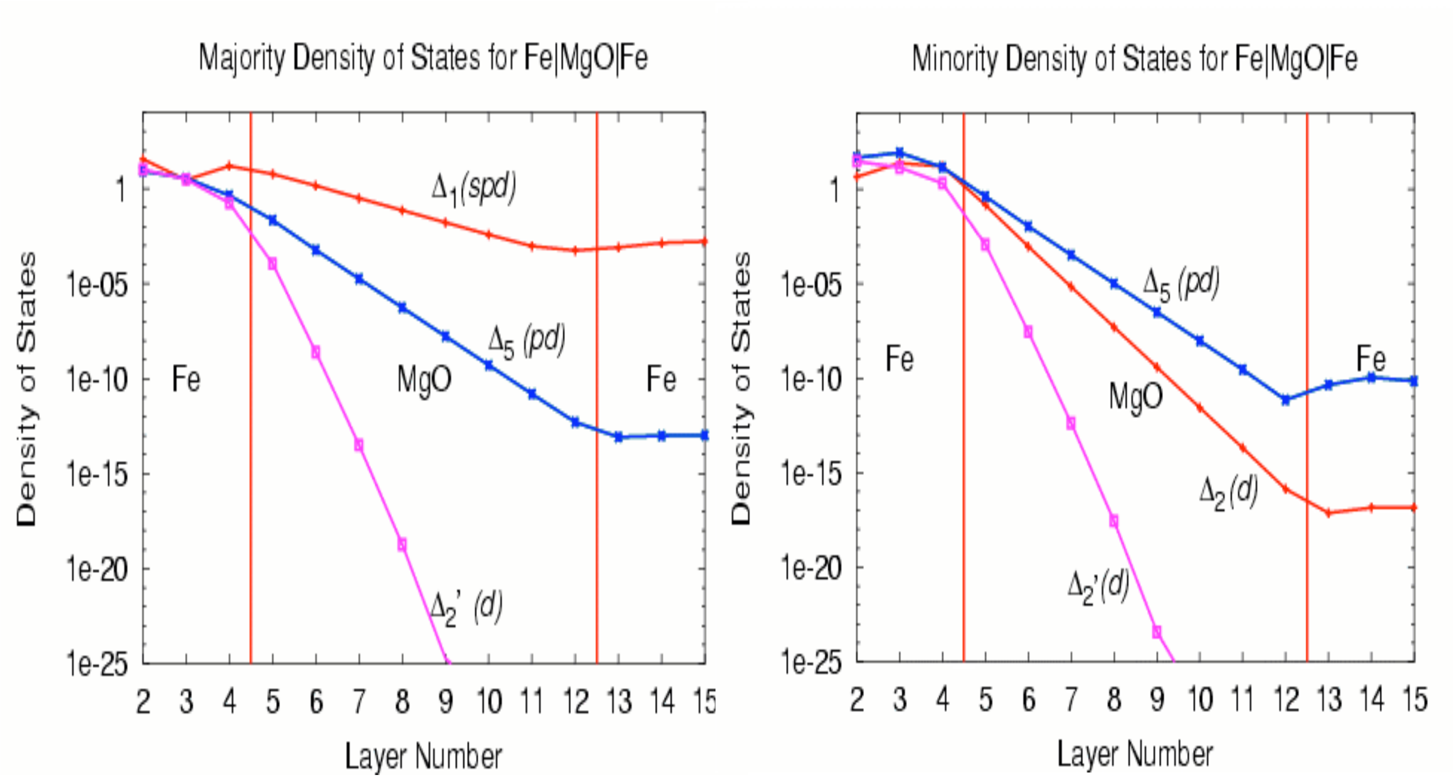

- *Majority channel tunneling is dominated by the transmission through a Δ_1 state.*
- *Minority spin Δ_5 state decays rapidly.*

WH Butler *et al Phys Rev B* **63** 054416 (2001)

Single MgO tunnel barrier

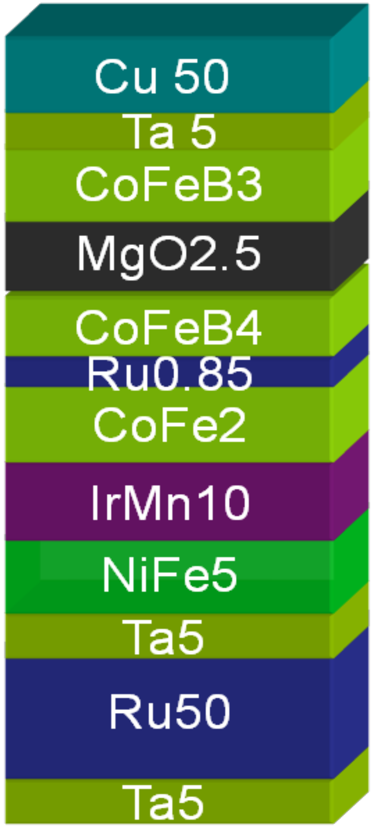

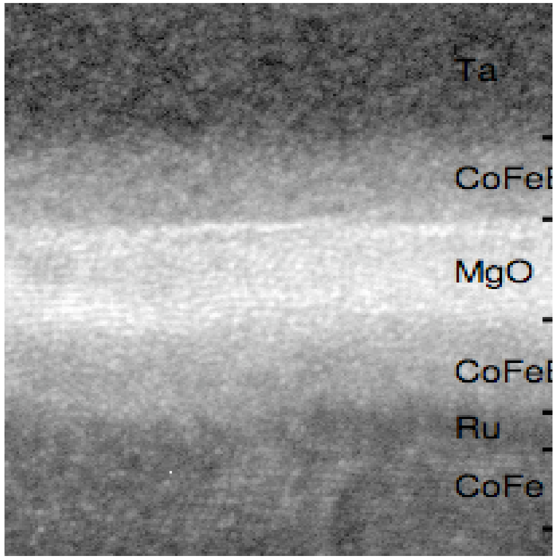

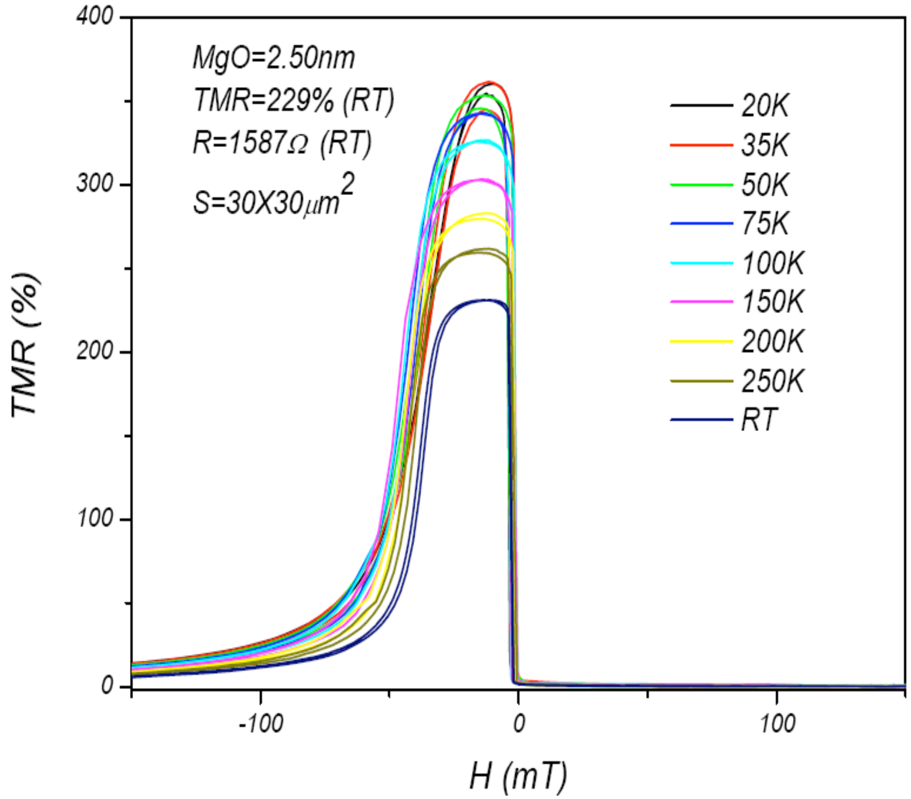

Amorphous CoFeB has to be crystallized in a post-deposition annealing step

I/f noise in MgO tunnel junctions

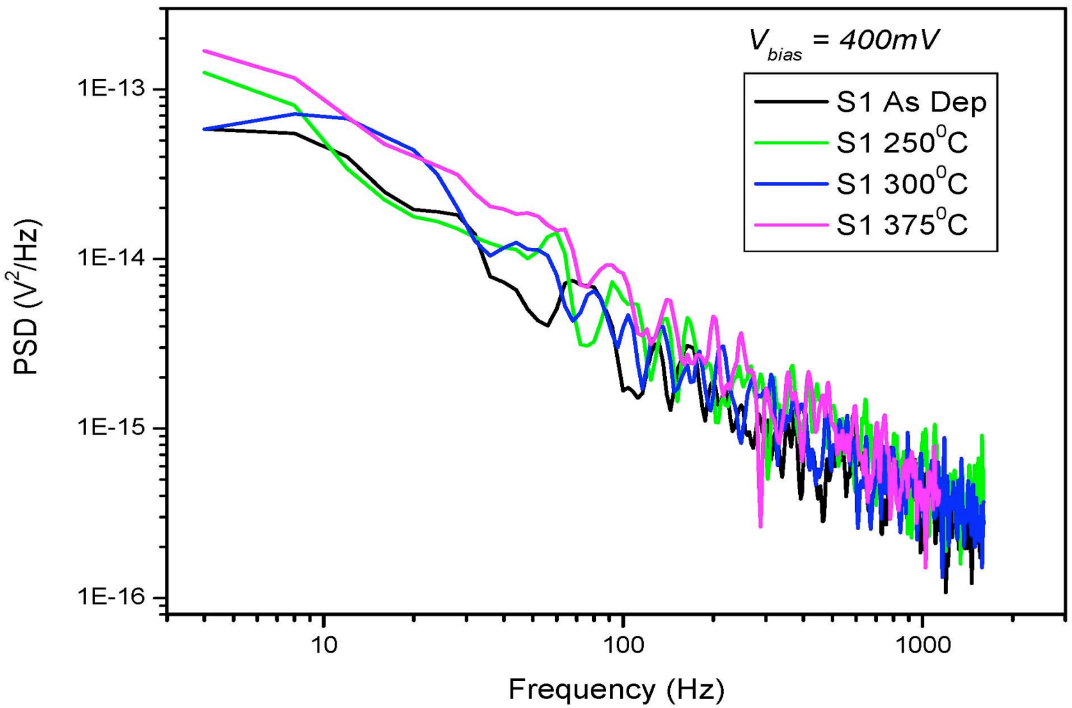

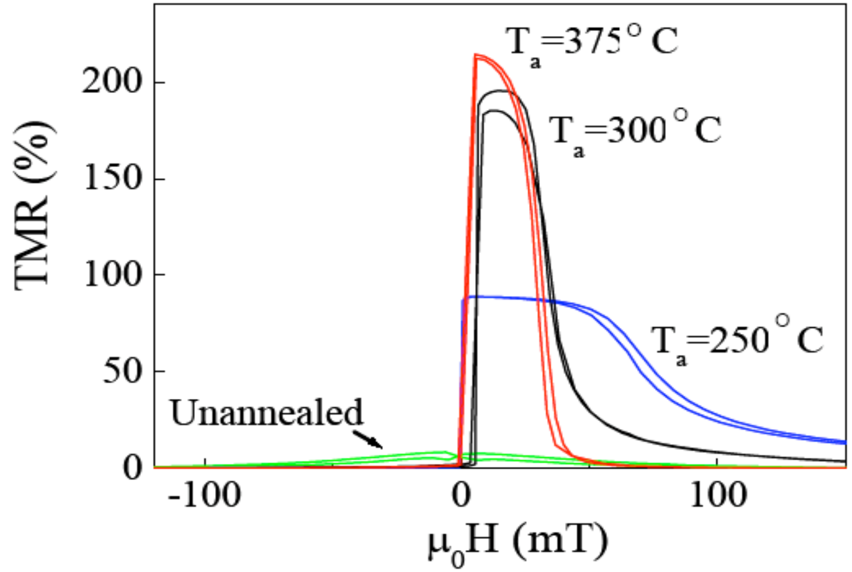

The I/f noise is independent of annealing temperature (TMR)

J. Schola *et al Appl.Phys Lett* **91** 102505 (2007)

1/f noise in MgO tunnel junctions

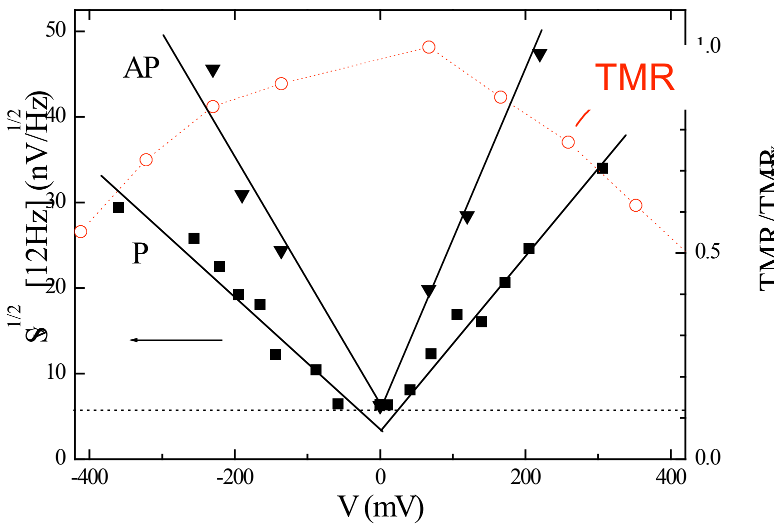

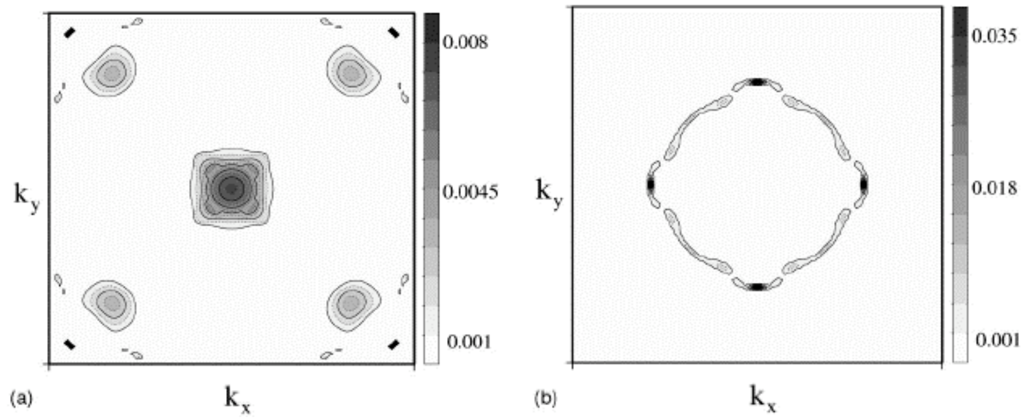

Partial conductance calculated for Fe/MgO/Fe junctions, MgO = 4 atomic plans

a) Γ_{major} k~0 **b) Γ_{minor} k≠0**

G. Mathon *et al.PRB* **63** 220403

$$\alpha = \frac{A\, f\, S_V(f)}{V^2}$$

$\alpha_{ap} > \alpha_p$

Majority carriers, Δ_1 $k \sim 0$. Little contribution to noise

Minority carriers, Δ_5 $k \neq 0$. Interaction with localized states in the barrier

MgO and AlO$_x$ barriers compared

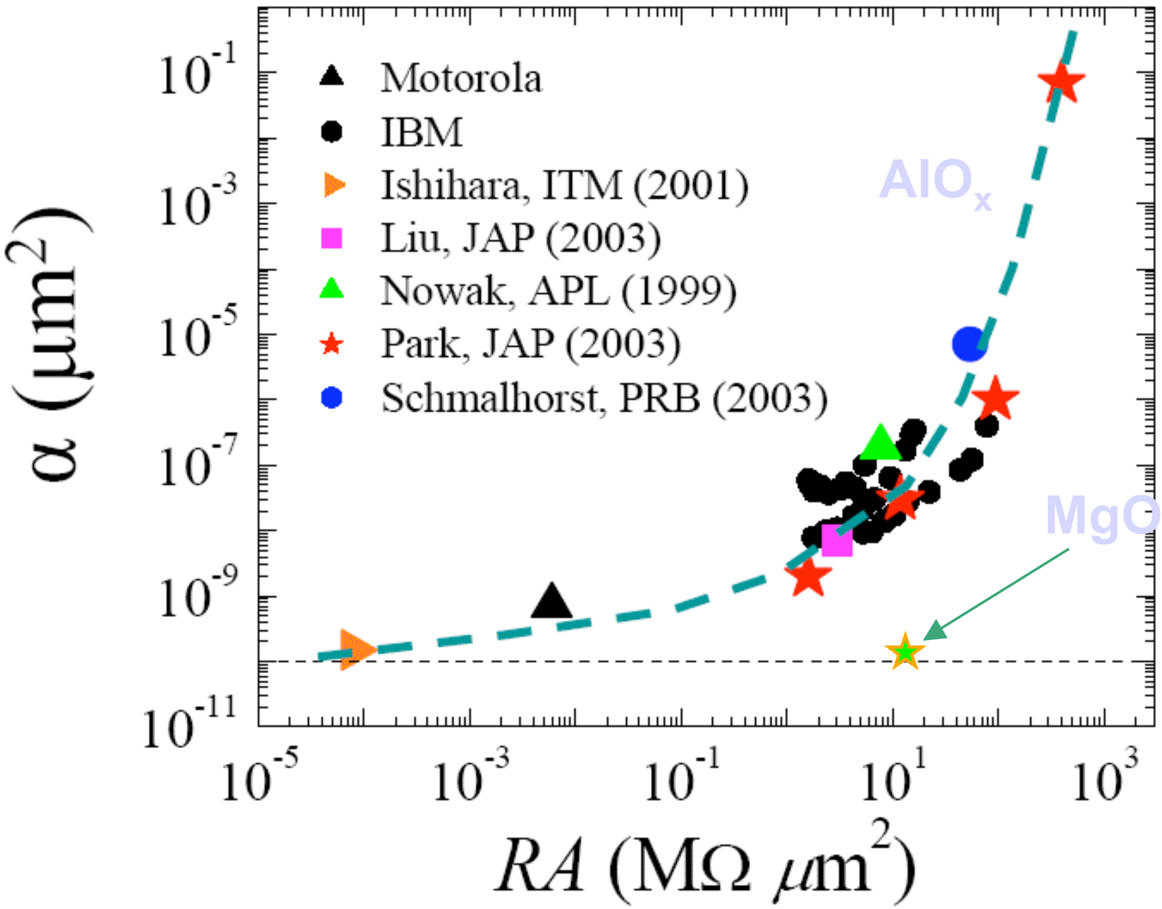

Figure from E.W. Nowak

α much lower with MgO than with Al_2O_3

Promising for applications

$\alpha_{4k} \sim \alpha_{300K}/100$

4.3.4 Giant magnetoimpedance.

GMI sensors are soft ferromagnetic wires (sometimes permalloy-plated copper wires} or films. An ac current is passed along the wire, and *L* is measured as a function of applied field. At high frequency, the skin depth < wire diameter. Permeability depends on *f* and *H*.

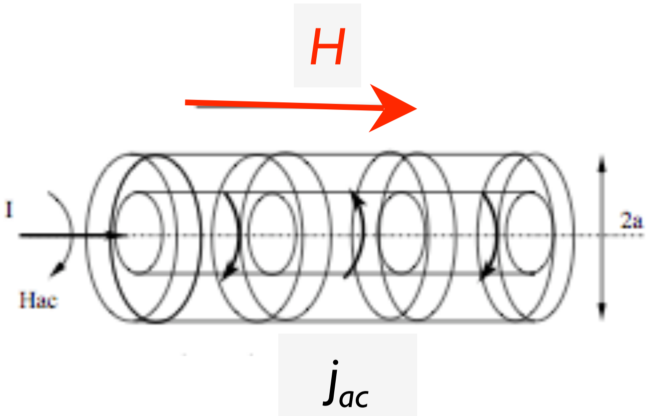

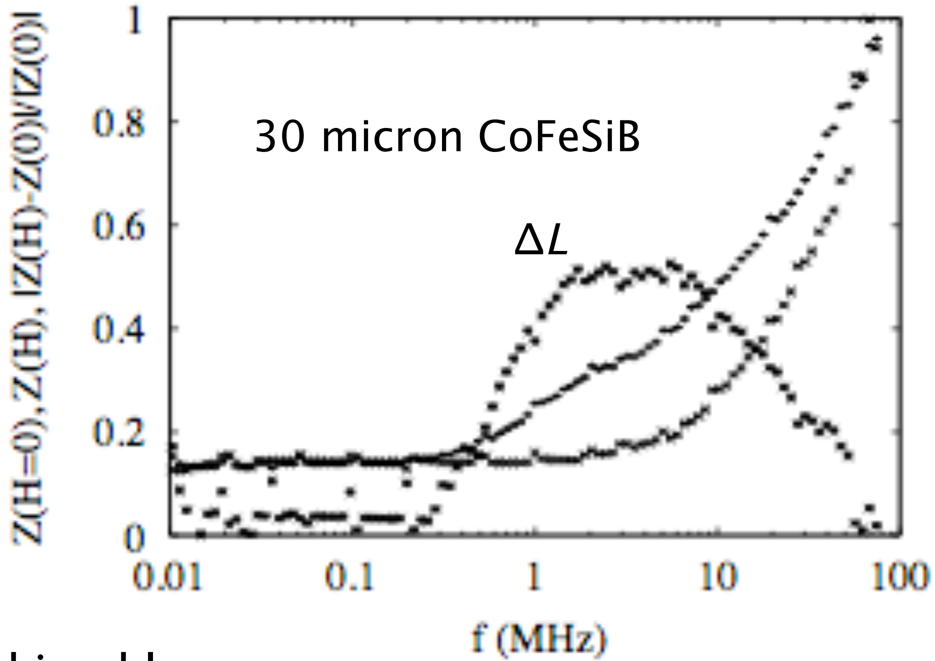

Very high field sensitivity, 10^4 % mT^{-1} is achievable
Used in Wii games, three-axis compasses …..